

# An assessment of the Arctic Ocean in a suite of interannual CORE-II simulations. Part I: Sea ice and solid freshwater

Qiang Wang<sup>a,\*</sup>, Mehmet Ilicak<sup>b</sup>, Rüdiger Gerdes<sup>a</sup>, Helge Drange<sup>c</sup>, Yevgeny Aksenov<sup>d</sup>, David A Bailey<sup>e</sup>, Mats Bentsen<sup>b</sup>, Arne Biastoch<sup>f</sup>, Alexandra Bozec<sup>g</sup>, Claus Böning<sup>f</sup>, Christophe Cassou<sup>h</sup>, Eric Chassignet<sup>g</sup>, Andrew C. Coward<sup>d</sup>, Beth Curry<sup>i</sup>, Gokhan Danabasoglu<sup>e</sup>, Sergey Danilov<sup>a</sup>, Elodie Fernandez<sup>h</sup>, Pier Giuseppe Fogli<sup>j</sup>, Yosuke Fujii<sup>k</sup>, Stephen M. Griffies<sup>l</sup>, Doroteaciro Iovino<sup>j</sup>, Alexandra Jahn<sup>e,m</sup>, Thomas Jung<sup>a,n</sup>, William G. Large<sup>e</sup>, Craig Lee<sup>i</sup>, Camille Lique<sup>o,p</sup>, Jianhua Lu<sup>g</sup>, Simona Masina<sup>j</sup>, A.J. George Nurser<sup>d</sup>, Benjamin Rabe<sup>a</sup>, Christina Roth<sup>f</sup>, David Salas y Mélia<sup>q</sup>, Bonita L. Samuels<sup>l</sup>, Paul Spence<sup>r,s</sup>, Hiroyuki Tsujino<sup>k</sup>, Sophie Valcke<sup>h</sup>, Aurore Voldoire<sup>q</sup>, Xuezhong Wang<sup>a</sup>, Steve G. Yeager<sup>e</sup>

<sup>a</sup>Alfred Wegener Institute, Helmholtz Centre for Polar and Marine Research (AWI), Bremerhaven, Germany

<sup>b</sup>Uni Research Ltd., Bergen, Norway

<sup>c</sup>University of Bergen, Bergen, Norway

<sup>d</sup>National Oceanography Centre (NOC), Southampton, SO14 3ZH, UK

<sup>e</sup>National Center for Atmospheric Research (NCAR), Boulder, CO, USA

<sup>f</sup>GEOMAR Helmholtz Centre for Ocean Research, Kiel, Germany

<sup>g</sup>Center for Ocean-Atmospheric Prediction Studies (COAPS), Florida State University, Tallahassee, FL, USA

<sup>h</sup>Centre Européen de Recherche et de Formation Avancée en Calcul Scientifique (CERFACS), Toulouse, France

<sup>i</sup>Applied Physics Laboratory, University of Washington, Seattle, Washington, USA

<sup>j</sup>Centro Euro-Mediterraneo sui Cambiamenti Climatici (CMCC), Bologna, Italy

<sup>k</sup>Meteorological Research Institute (MRI), Japan Meteorological Agency, Tsukuba, Japan

<sup>l</sup>NOAA Geophysical Fluid Dynamics Laboratory (GFDL), Princeton, NJ, USA

<sup>m</sup>Department of Atmospheric and Oceanic Sciences, University of Colorado, Boulder, CO, USA

<sup>n</sup>Institute of Environmental Physics, University of Bremen, Bremen, Germany

<sup>o</sup>Department of Earth Sciences, University of Oxford, Oxford, UK

<sup>p</sup>Laboratoire de Physique des Océans, Ifremer, centre de Brest, Plouzané, France

<sup>q</sup>Centre National de Recherches Météorologiques (CNRM), Toulouse, France

<sup>r</sup>Climate Change Research Centre, University of New South Wales, Sydney, Australia

<sup>s</sup>ARC Centre of Excellence for Climate System Science, University of New South Wales, Sydney, Australia

---

## Abstract

The Arctic Ocean simulated in fourteen global ocean-sea ice models in the framework of the Coordinated Ocean-ice Reference Experiments, phase II (CORE II) is analyzed. The focus is on the Arctic sea ice extent, the solid freshwater (FW) sources and solid freshwater content (FWC). Available observations are used for model evaluation. The variability of sea ice extent and solid FW budget is more consistently reproduced than their mean state in the models. The descending trend of September sea ice extent is well simulated in terms of the model ensemble mean. Models overestimating sea ice thickness tend to underestimate the descending trend of September sea ice extent. The models underestimate the observed sea ice thinning trend by a factor of two. When averaged on decadal time scales, the variation of Arctic solid FWC is contributed by both sea ice production and sea ice transport, which are out of phase in time. The solid FWC decreased in the recent decades, caused mainly by the reduction in sea ice thickness.

*Keywords:* Arctic Ocean, Sea ice, Freshwater, CORE II atmospheric forcing

---

## Contents

<b>1</b>	<b>Introduction</b>	<b>2</b>
1.1	Participating models . . . . .	3
1.2	Basic concepts . . . . .	4

---

\*Corresponding author

Email address: Qiang.Wang@awi.de (Qiang Wang)

5	1.3 Model spin-up . . . . .	6
	<b>2 Sea ice extent and concentration</b>	<b>7</b>
	2.1 Mean state . . . . .	7
	2.2 Variability and trend . . . . .	7
	2.3 Sea ice extent in Barents Sea . . . . .	11
10	2.4 Summary on the model ensemble mean of sea ice extent . . . . .	13
	<b>3 Solid freshwater</b>	<b>14</b>
	3.1 Mean state . . . . .	14
	3.1.1 Solid freshwater sources . . . . .	14
	3.1.2 Solid freshwater content . . . . .	15
15	3.2 Interannual Variability and trend . . . . .	18
	3.2.1 Solid freshwater sources . . . . .	18
	3.2.2 Solid freshwater content . . . . .	21
	3.3 Seasonal variability . . . . .	23
	3.4 Summary on the model ensemble mean of solid FW . . . . .	26
20	<b>4 Conclusion</b>	<b>27</b>
	<b>Appendix A. Definition of freshwater content and transport</b>	<b>29</b>
	<b>Appendix B. Model spinup</b>	<b>30</b>
	<b>References</b>	<b>34</b>

## 1. Introduction

25 The Arctic Ocean is an important component of the climate system. It closely interacts with the atmosphere at the surface and is connected with the large scale ocean circulation through its gateways. Sea ice, a unique feature of the high latitude oceans, modifies the planetary albedo and impacts on the air-sea heat, momentum, mass and gas exchange. Arctic sea ice has retreated significantly in recent years (Kwok and Rothrock, 2009; Comiso, 2012; Cavalieri and Parkinson, 2012; Stroeve et al., 2012a; Laxon et al., 2013), causing amplified warming in the Arctic region (Serreze and Barry, 2011) and far-reaching impact on the Earth System (Bhatt et al., 2014). The Arctic Ocean is a large freshwater (FW) reservoir due to river runoff, net precipitation (P-E) and FW import from the Pacific (Serreze et al., 2006; Dickson et al., 2007). The excess FW is exported to the subpolar North Atlantic, which can influence the upper ocean stratification and deep water formation, and thus the meridional overturning circulation (e.g., 30 Aagaard et al., 1985; Goosse et al., 1997; Hakkinen, 1999; Wadley and Bigg, 2002; Jungclaus et al., 2005). At depth the intermediate water leaves the Arctic Ocean through Fram Strait, supplying dense waters that overflow into the Atlantic proper and then feed the North Atlantic Deep Water (Rudels and Friedrich, 2000; Karcher et al., 2011). Because of its essential role in the climate system, understanding the functioning of the Arctic Ocean and predicting its future are among the key topics of climate research.

40 Improved understanding of the Arctic Ocean has been achieved by using both observations and numerical simulations (see reviews by Proshutinsky et al., 2011; Haine et al., 2015). As model uncertainty can impact on the robustness of both physical mechanisms and climate changes inferred from model simulations, assessment of model performance is necessary. Model intercomparison is a useful method to illustrate model consistency and spread, thus helping to identify required model improvements. Model intercomparisons for the Arctic Ocean have been carried out based on both coupled climate models (e.g., Holland et al., 2007; Rawlins et al., 2010; Stroeve et al., 2012a) and forced ocean-ice models (e.g., Holloway et al., 2007; Karcher et al., 2007; Johnson et al., 2007; Jahn et al., 2012a; Johnson et al., 2012). The latter studies are based on models participating in the Arctic Ocean Model Intercomparison Project (AOMIP, Proshutinsky et al., 2011).

50 In this work we analyze and compare the ocean and sea ice properties in the Arctic Ocean simulated by models participating in the Coordinated Ocean-ice Reference Experiments, phase II (CORE-II) project. Model intercomparison under the CORE-II framework has a few advantages. First, all ocean-ice models

are driven by the same atmospheric state, the CORE interannual forcing (Large and Yeager, 2009), and use the same (NCAR) bulk formulae (see the CORE-II protocol described by Griffies et al. (2012)). A common atmospheric state helps isolate model-dependent uncertainty from that induced by different atmospheric states. Second, all participating models are *global* ocean-ice models, which have been used in different coupled climate models. Many of these climate models have participated in the Climate Model Intercomparison Project (CMIP). Model (in)consistency diagnosed from these ocean-ice models can provide information not only to Arctic researchers, but also to climate model developers for improving their Arctic Ocean components. Third, model intercomparisons for different topics and regions of the world ocean are done in parallel under the CORE-II framework (see other papers in this special issue). The combination of these studies will provide an overall view on the current status of global ocean-ice models used in climate research. We hope that the joint efforts can provide information useful to improve overall climate model integrity.

Our focus in the CORE-II Arctic framework is on the Arctic sea ice extent and concentration, the solid and liquid FW budget, and the Arctic intermediate water layer. We discuss which characteristics are more consistently simulated in the models and what common issues exist among them. Comparisons are made to available observations. We will compare and discuss the simulated properties, but their impact on the large scale circulation is beyond the scope of this work.

During the course of preparing the manuscript, we recognize that some model developers and users, in particular those just starting to analyze their simulated Arctic results in global models, find the preliminary version of the paper very useful. They use it as a compact introduction to the Arctic Ocean modelling, taking from it the information on, for example, what results can be expected from the state-of-the-science ocean climate models. We are encouraged by the feedbacks, so we try to present the model comparison with a broad view including the three major Arctic topics mentioned above. This is in line with the pedagogic aspect of the CORE project. In order to maintain the readability we split the content into three papers. This paper deals with Arctic sea ice extent and solid freshwater. The other two papers focus on the Arctic liquid freshwater (Wang and et al., 2015) and the hydrography in the Arctic Ocean (Ilicak and et al., 2015).

### 1.1. Participating models

Table 1: Summary of the ocean and sea-ice models in alphabetical order according to the participating group name (first column). The table includes the name of the combined ocean-sea ice configuration (if any); the ocean model name and its version; the sea-ice model name and its version; vertical coordinate and number of layers/levels in parentheses; orientation of the horizontal grid with respect to the North Pole/Arctic; the number of horizontal grid cells (longitude, latitude); and the horizontal resolution (longitude, latitude). In MRI-A and MRI-F, the vertical levels shallower than 32 m follow the surface topography as in sigma-coordinate models. In AWI-FESOM, the total number of surface nodes is given, because it has an unstructured grid. The suite of participating models include 13 models analyzed in the CORE-II North Atlantic paper (Danabasoglu et al., 2014), and one 0.25° fine horizontal grid spacing model (MOM0.25). FSU-HYCOM has a new model version for the CORE-II study (Danabasoglu et al., 2015), but it is not included in this work.

Group	Configuration	Ocean model	Sea-ice model	Vertical	Orientation	Horiz. grid	Horiz. res.
AWI		FESOM 1.4	FESIM	z (46)	Displaced	126000	Nominal 1°
Bergen	NorESM-O	MICOM	CICE 4	$\sigma_2$ (51+2)	Tripolar	360 × 384	Nominal 1°
CERFACS	ORCA1	NEMO 3.2	LIM 2	z (42)	Tripolar	360 × 290	Nominal 1°
CMCC	ORCA1	NEMO 3.3	CICE 4	z (46)	Tripolar	360 × 290	Nominal 1°
CNRM	ORCA1	NEMO 3.2	Gelato 5	z (42)	Tripolar	360 × 290	Nominal 1°
FSU		HYCOM 2.2	CSIM 5	hybrid (32)	Displaced	320 × 384	Nominal 1°
GFDL-MOM	ESM2M-ocean-ice	MOM 4p1	SIS1	z* (50)	Tripolar	360 × 200	Nominal 1°
GFDL-UNSW	MOM0.25	MOM 5	SIS1	z* (50)	Tripolar	1440 × 1070	Nominal 0.25°
GFDL-GOLD	ESM2G-ocean-ice	GOLD	SIS1	$\sigma_2$ (59+4)	Tripolar	360 × 210	Nominal 1°
Kiel	ORCA05	NEMO 3.1.1	LIM 2	z (46)	Tripolar	722 × 511	Nominal 0.5°
MRI-A	MRI assimilation	MOVE/MRI.COM 3	MK89; CICE	z (50)	Tripolar	360 × 364	1° × 0.5°
MRI-F	MRI free run	MRI.COM 3	MK89; CICE	z (50)	Tripolar	360 × 364	1° × 0.5°
NCAR		POP 2	CICE 4	z (60)	Displaced	320 × 384	Nominal 1°
NOC	ORCA1	NEMO 3.4	LIM 2	z (75)	Tripolar	360 × 290	Nominal 1°

Data from fourteen CORE-II models are analyzed in this paper. Thirteen of them were described in

the first CORE-II paper focused on the North Atlantic (Danabasoglu et al., 2014)<sup>1</sup>. One new model is the global 0.25° MOM. Adding it to the analysis serves to provide information on how fine horizontal grid spacing can influence simulation results. The models are listed in Table 1, together with the groups names operating the models and the basic model configuration information. Seven different sea ice models are used in the fourteen ocean-ice models. Most of the models use z-level (or z\*) coordinates, except for three models with isopycnal or hybrid vertical grids (GOLD, FSU and Bergen). One model is an unstructured-mesh model (AWI-FESOM), configured with traditional climate model resolution for the purpose of the CORE-II project. Among the participating models, ten models have nominal 1° horizontal resolution, three with 0.5°, and one with 0.25°. The resolution in km varies significantly in space and direction in the Arctic Ocean, so we can only give very approximate mean values. MOM0.25 has about 12 km horizontal resolution, Kiel-ORCA05 and FESOM have about 24 km, and the other models have about 48 km.

One of the participating models, MRI-A, is a global ocean data assimilation system. It is the same as MRI-F except that temperature and salinity observational data are assimilated into the model. It was run for 70 years starting from model year 231 of the MRI-F integration. The first 10 years are treated as a spin-up phase and the last 60 years (associated with the period of CORE-II forcing) are used in this work. Its results are compared to other models to provide information on whether the assimilation improves the key diagnostics of the Arctic Ocean. However, *we do not include it for calculating model ensemble means*.

As discussed by Griffies et al. (2009), ocean-ice models without a coupled active atmospheric model lack many of the feedbacks present in a fully coupled system. This necessitates restoring of model sea surface salinity (SSS) to observed climatological SSS in global ocean-ice models. In addition, SSS restoring helps to avoid unbounded local salinity trends that can occur in response to inaccuracies in precipitation. The strength of SSS restoring (defined by a piston velocity) is not specified in the CORE-II protocol and left to modellers to choose. The details of SSS restoring methods and piston velocity used in the models are described in Appendix C and Table 2 in Danabasoglu et al. (2014)<sup>2</sup>. It is worth mentioning here that SSS restoring is turned off under sea ice in Kiel-ORCA05. It will serve as a reference for the discussion of the potential impact of SSS restoring on the Arctic liquid FW budget.

In this paper we define the Arctic Ocean domain with the following four gateways: Bering Strait, Fram Strait, Davis Strait, and the Barents and Kara Seas northern boundary (BKN) (see Figure 1). Bering Strait is the only gateway connecting the Arctic Ocean with the Pacific. In the Atlantic sector, the Arctic Ocean is connected with the Nordic Seas via Fram Strait, with the Labrador Sea via Davis Strait, and with the Barents/Kara Seas then the Nordic Seas via the BKN. We take Davis Strait rather than the Canadian Arctic Archipelago (CAA) as one of the Arctic Ocean boundaries for simplicity because the number of CAA passages connecting the Arctic Ocean and Baffin Bay is different among the models.

Tables 1 shows the basic model configurations, therein we list the models in the alphabetical order with respect to the names of the contributing groups. In all figures and other tables in this paper, we will group the models according to types of vertical coordinates and model origins, when possible. The five models based on NEMO are put closer, the same for the two MOM models with different horizontal resolution, the three isopycnal (and hybrid) models, and the free-run and assimilated MRI models.

## 1.2. Basic concepts

*Sea ice extent.* The decline of Arctic sea ice, with possible impact on different components of the Earth System (Bhatt et al., 2014), has emerged as a leading signal of global warming. The mean state and decline of sea ice need to be quantified, often by using the so-called sea ice extent, which is defined as *the sum of ice covered areas with sea ice concentrations of at least 15%*. The sea ice concentration is the fractional area of the ocean covered by sea ice.

---

<sup>1</sup>The analysis done for this paper discovered a bug in the CERFACS NEMO model. The NEMO grid is folded at the North Pole for an entire grid line going from Canada to Asia at 78°W. On this specific grid line, the wind forcing fields need to be rotated onto the local grid coordinates. This is not correctly done in the CERFACS simulation, leading to spurious signals in ice dynamical fields (e.g., as shown by the sea ice concentration in Figure 4). It is found that this bug has a very local imprint and did not significantly influence the freshwater budget analyzed in this work.

<sup>2</sup>The actually used piston velocity (50 m over 100 days) in the CNRM model is stronger than that indicated in Danabasoglu et al. (2014).

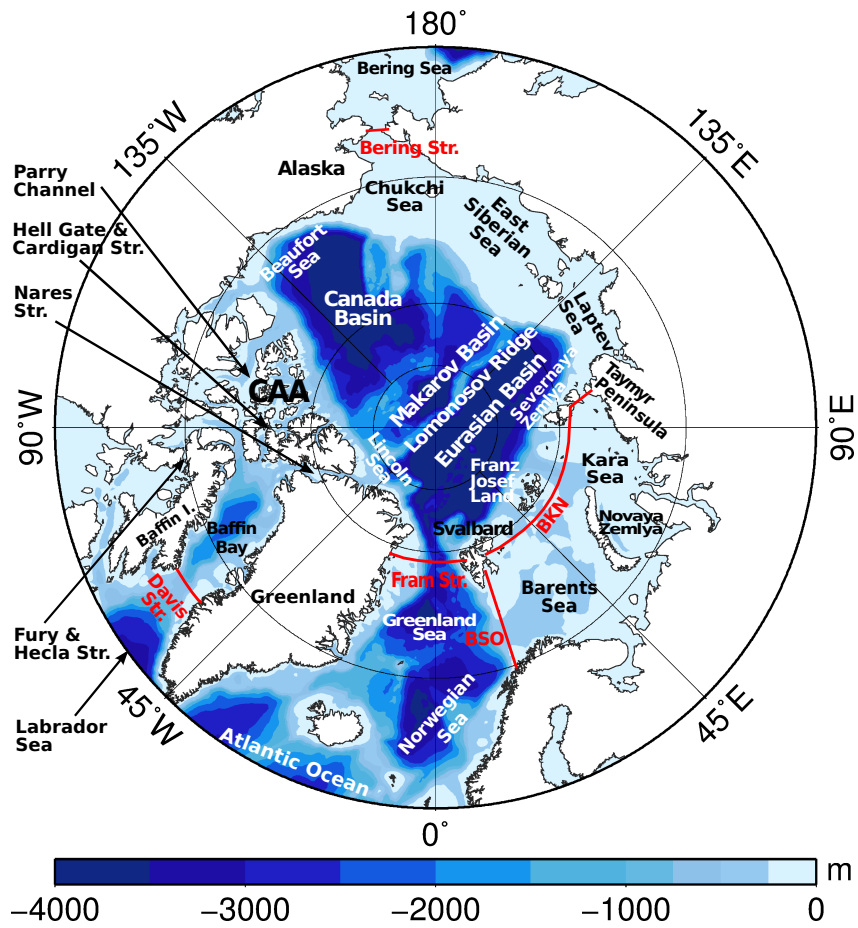


Figure 1: Arctic Ocean bottom topography [m]. The Arctic gateways discussed in the paper are shown with red lines. BSO stands for southern Barents Sea Opening, BKN for Barents/Kara Seas northern boundary, and CAA for Canadian Arctic Archipelago.

Sea ice area, the summed product of the ice concentration and area of each data element within the ice extent, is another widely used quantity for describing sea ice cover. In this work we only assess the simulated sea ice extent, and note that the descending trends of Arctic sea ice extent and area are different, especially when compared for particular regions and seasons (Cavalieri and Parkinson, 2012; Comiso, 2012).

For evaluating the sea ice extent, we compare both the simulated mean state and trend with satellite observations (Fetterer et al., 2002). The comparison is made for September and March when the Northern Hemisphere (NH) sea ice extent has minimum and maximum, respectively (note that the maximal and minimal descending trends are in September and May, respectively, for the period of 1979 - 2010 (Cavalieri and Parkinson, 2012)). In addition to the total NH sea ice extent, we also evaluate the models for one chosen region, the Barents Sea, where most significant sea ice retreat is predicted in simulations of future climate (Koenigk et al., 2013).

*Arctic freshwater.* The Arctic Ocean is a big FW reservoir (Serreze et al., 2006; Dickson et al., 2007). It receives FW as river runoff, precipitation and inflow from Bering Sea. The amount of FW stored in the Arctic Ocean is an important index that can be used to describe the climate status of the Arctic Ocean. The excess FW received by the Arctic Ocean is finally released to the North Atlantic through Fram and Davis Straits. Due to the proximity to the deep water formation sites and potential impact on large scale ocean circulation (Dickson et al., 1988; Goosse et al., 1997; Hakkinen, 2002; Wadley and Bigg, 2002), the FW flux from the Arctic Ocean to the North Atlantic is one of the key variables describing the linkage between the Arctic and subpolar regions.

FW in the Arctic Ocean exists in the solid form mainly as sea ice and in the liquid form mainly located in the upper ocean. We call sea ice and particular ocean waters *FW* because their salinity is lower than a *reference* value, which is chosen according to the context of discussed topics. For example, if one wants to study the impact of Arctic FW export on the deep water formation in the North Atlantic, she/he will take the mean salinity of the subpolar North Atlantic as the reference salinity; if one analyzes the FW budget in the Arctic Ocean, she/he might choose a value representing the mean state of the Arctic Ocean. In this paper we focus on the Arctic region, so we take 34.8, a value close to the mean salinity in the Arctic basins as the reference salinity following Aagaard and Carmack (1989) and Serreze et al. (2006). Using this common value allows us to compare the model results directly with the synthesized Arctic FW budget (Serreze et al., 2006; Haine et al., 2015) and analyses in many observational and model studies<sup>3</sup>.

Understanding the Arctic FW budget involves quantifying both the Arctic FW storage and sources, including fluxes through the gateways. The FW storage in the Arctic Ocean can be quantified using the so-called freshwater content (FWC), which is *the amount of zero-salinity water required to be taken out from the ocean (or sea ice) so that the ocean (or sea ice) salinity is changed to the chosen reference salinity*. The FW flux through a gateway is similarly defined as the equivalent flux of zero-salinity water. See Appendix A for how the FWC and FW fluxes are calculated. When we evaluate the Arctic FW storage and sources, we will focus on three aspects: mean state, interannual changes and seasonal variability, and the model ensemble means are also assessed at the end of each section.

### 1.3. Model spin-up

The CORE-II atmospheric state used to drive the models covers 60 years from 1948 to 2007 (Large and Yeager, 2009). All models are run for 300 years, corresponding to 5 consecutive loops of the 60-year forcing period following the CORE-II protocol (Griffies et al., 2012). In the CORE-II model intercomparison for the North Atlantic, it was shown that 5 loops are sufficient for more than half of the models to reach equilibrium with respect to the key diagnostic, the Atlantic Meridional Overturning Circulation (AMOC) maximum (Danabasoglu et al., 2014). In Appendix B the spin-up of the ocean in terms of two important diagnostics (Arctic liquid FWC and FW flux to the North Atlantic) is evaluated. It is shown that most of the models reach a good equilibrium state at the end of the experiment for the Arctic Ocean.

Because the Arctic sea ice retreats in the recent decades and each model loop starts from the end of the preceding loop, the simulated Arctic Ocean experiences vigorous adjustment at the beginning

---

<sup>3</sup>Note that slightly different reference salinity values have also been used in literature.

180 of each loop. For example, the low sea ice extent and thickness at the end of 2007 increases after the  
atmospheric state is changed back to 1948 in the next model loop. When discussing the model results,  
we only take the last 30 model years of the 5th model loop, if not otherwise mentioned. The period is  
relatively short, but this choice helps to reduce the influence of the loop to loop adjustment, although  
185 the choice is somewhat arbitrary as we do not know exactly how long the adjustment can affect the  
ocean-ice system. Observations available for model evaluation are concentrated in the period of the last  
three model decades, which is another reason for us to focus on this period. Although our discussion  
focuses mainly on the last 30 years, in most of the plots of time series in this paper we show the whole  
5th loop because the information can be useful for readers who are interested in a longer time period.

190 The paper is organized as follows. First we discuss sea ice extent and concentration in Section 2,  
then the solid FW budget is assessed in Section 3. The concluding remarks are given in Section 4.

## 2. Sea ice extent and concentration

Continuous satellite observation of sea ice concentration started in 1979. This observation period is  
characterized by a significant decline of the Arctic sea ice cover (Parkinson et al., 1999; Serreze et al., 2007;  
Comiso and Nishio, 2008; Parkinson and Cavalieri, 2008). The sea ice retreat continued to accelerate  
195 in the recent decade, the most strongly in September (Stroeve et al., 2012b; Cavalieri and Parkinson,  
2012; Comiso, 2012). A few September sea ice extent minima have been observed since 2002. A record  
minimum was seen in 2005, and then the Arctic sea ice extent in September 2007 fell to a lower value,  
more than 20% below the 2005 minimum (Comiso et al., 2008; Stroeve et al., 2008).<sup>4</sup> The accelerated  
sea ice retreat involves a suite of linked processes including increasing air temperature and enhanced  
200 ice-albedo feedback (Stroeve et al., 2012b), and contributes to amplified Arctic warming (Serreze and  
Barry, 2011).

Due to its crucial roles in the climate system, the status of sea ice is among the key model variables  
that need to be evaluated. In this section we assess the Northern Hemisphere (NH) sea ice extent and  
concentration simulated in the CORE-II models by comparing to the satellite observations, which are  
205 regularly updated (Fetterer et al., 2002). The mean state and trend of NH sea ice extent is discussed  
in Section 2.1 and 2.2, respectively. The Arctic sea ice declines regionally at different rates (Cavalieri  
and Parkinson, 2012), so it is also interesting to assess the simulated sea ice on a regional basis. In  
this paper we do not attempt to compare all the Arctic regions, and only focus on one particular shelf  
sea, the Barents Sea, where most significant sea ice retreat is predicted in simulations of future climate  
210 (Koenigk et al., 2013). This is presented in Section 2.3. A summary on the model ensemble mean is  
given in Section 2.4.

### 2.1. Mean state

The modelled NH sea ice extent in the last model loop is shown in Figure 2 together with the NSIDC  
observation (Fetterer et al., 2002). In both September and March, the simulated NH sea ice extent  
215 among the models is spread around the observed values. We define the model spread as the standard  
deviation of the mean sea ice extent. The model spread in September is about 26% of the observed  
mean sea ice extent, much larger than the spread in March (see Table 2). The growth of sea ice extent  
in freezing seasons is confined by the continents around the Arctic Ocean, which can partly explain the  
smaller model spread in March. The September sea ice extent is overestimated in five models (AWI-  
220 FESOM, CERFACS, Kiel-ORCA05, NOC and MRI-F), and significantly underestimated in four models  
(NCAR, CMCC, FSU-HYCOM, Bergen). In the latter four models, the September sea ice extent drops  
to anomalously low levels already at the end of the 1990s. Except for these four models, all other models  
produced lowest September sea ice extent in 2007 in the model integration period, in agreement with  
the observation.

### 2.2. Variability and trend

The strength of interannual variability, represented by the standard deviation of monthly time series,  
is stronger in September than in March in the observation and the models (Table 2). In September,

---

<sup>4</sup>So far the lowest Arctic sea ice extent was observed in September 2012, beyond the period of model integration.

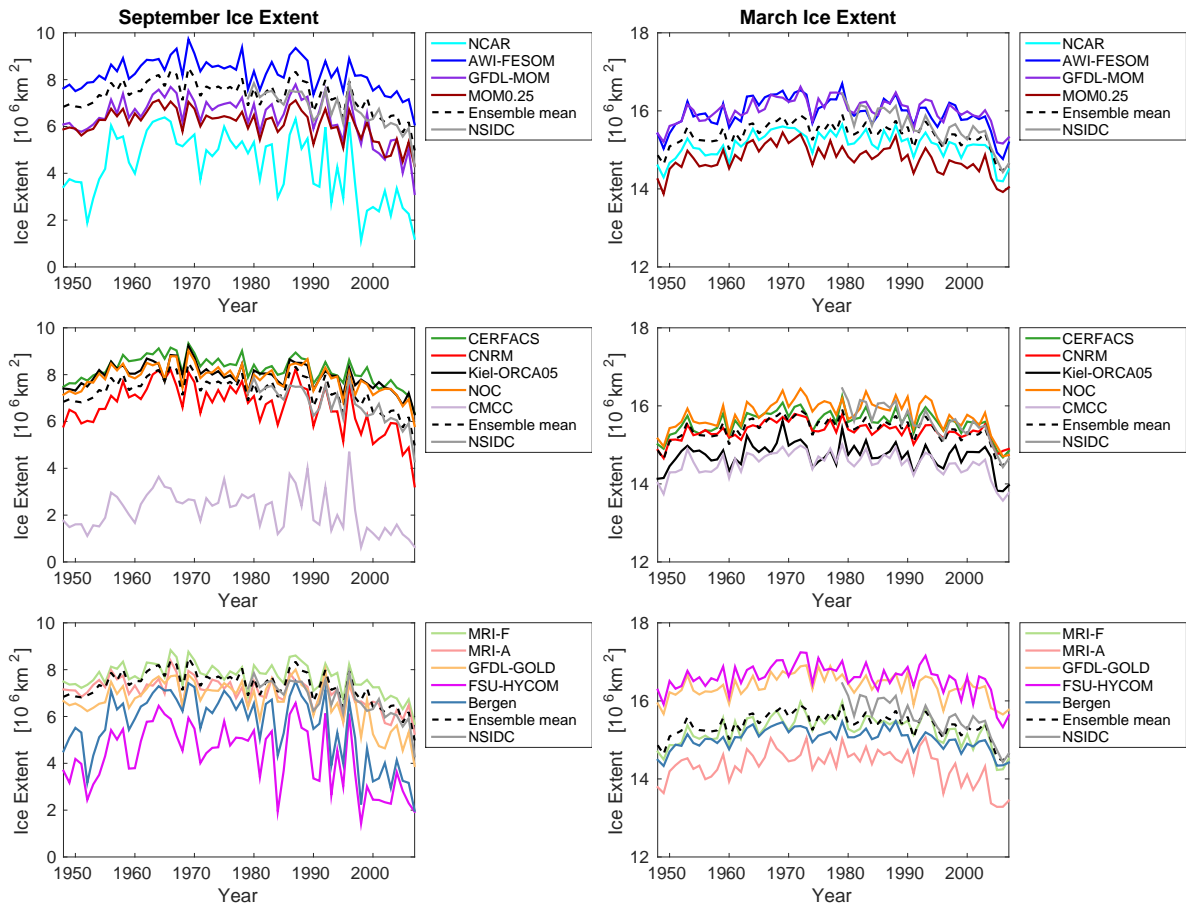


Figure 2: Northern Hemisphere (left) September and (right) March sea ice extent [ $10^6 \text{km}^2$ ] in the last model loop. Note that the assimilation model MRI-A is not used in the calculation of the model ensemble mean. The observation from NSIDC (Fetterer et al., 2002) is shown with gray lines for the period of 1979-2007.

Table 2: Northern Hemisphere (NH) sea ice extent: mean, standard deviation (STD), correlation with observation, linear trend, and the 2007 value. The last two columns show the model ensemble mean and spread.<sup>1</sup>

	Observation	NCAR	AWI	MOM	MOM0.25	CERFACS	CNRM	Kiel	NOC	CMCC	MRI-F	MRI-A	GOLD	FSU	Bergen	mean	spread
September																	
mean	6.95	3.99	8.18	6.30	5.96	8.12	6.46	7.85	7.76	2.14	7.65	6.84	6.52	4.00	5.27	6.17	1.87
STD	0.58	1.44	0.61	0.89	0.66	0.42	0.86	0.43	0.49	1.04	0.57	0.61	0.98	1.54	1.47	0.88	0.40
correlation		0.71	0.76	0.63	0.73	0.67	0.67	0.74	0.64	0.68	0.79	0.80	0.62	0.72	0.60	0.69	0.06
trend 79-03	-5.3	-11.0	-2.7	-6.4	-4.4	-2.5	-5.9	-2.1	-2.6	-5.2	-3.5	-4.2	-7.5	-10.9	-12.8	-6.0	3.6
trend 79-07	-7.2	-11.3	-4.9	-8.9	-5.5	-4.3	-8.5	-3.9	-4.5	-6.0	-5.4	-4.9	-9.0	-10.4	-13.6	-7.2	3.0
2007 ice extent	4.30	1.21	6.09	3.12	4.31	6.34	3.23	6.31	5.80	0.64	5.69	5.26	3.89	1.93	1.98	3.89	2.04
March																	
mean	15.72	15.20	15.98	16.06	14.78	15.66	15.38	14.78	15.87	14.57	15.33	14.43	16.40	16.60	15.06	15.51	0.64
STD	0.34	0.22	0.25	0.22	0.24	0.21	0.15	0.24	0.28	0.20	0.29	0.38	0.24	0.29	0.21	0.24	0.04
correlation		0.65	0.66	0.60	0.76	0.59	0.76	0.65	0.46	0.80	0.45	0.37	0.68	0.21	0.67	0.61	0.16
trend 79-03	-3.4	-1.4	-1.3	-1.1	-1.6	-1.3	-0.7	-0.9	-1.8	-1.2	-2.1	-3.3	-0.9	-1.3	-1.7	-1.3	0.4
trend 79-07	-4.7	-2.7	-3.1	-2.5	-2.8	-2.7	-1.7	-2.3	-3.5	-2.7	-3.5	-4.8	-2.2	-3.1	-2.6	-2.9	0.7
2007 ice extent	14.65	14.50	15.19	15.32	14.04	14.85	14.90	13.97	14.74	13.77	14.52	13.45	15.77	15.63	14.42	14.74	0.62

<sup>1</sup> Sea ice extent is in  $10^6 \text{km}^2$ , and the trend is in  $10^4 \text{km}^2/\text{year}$ . The statistics are calculated for September and March monthly data separately. The last few years feature more rapid sea ice retreat, so we use the years 1979 - 2003 in the calculation of the sea ice extent, its standard deviation (STD), correlation with the observation, and the linear trend. The correlation coefficients are calculated after the linear trend is removed. The observation is based on the sea ice index provided by Fetterer et al. (2002). Note that the assimilation model MRI-A is not used in the calculation of the model ensemble mean and spread, the same as in other tables and figures. The linear trend for the whole period (1979-2007) is also shown in the table; it compares with the observation better than for the shorter period (1979-2003).

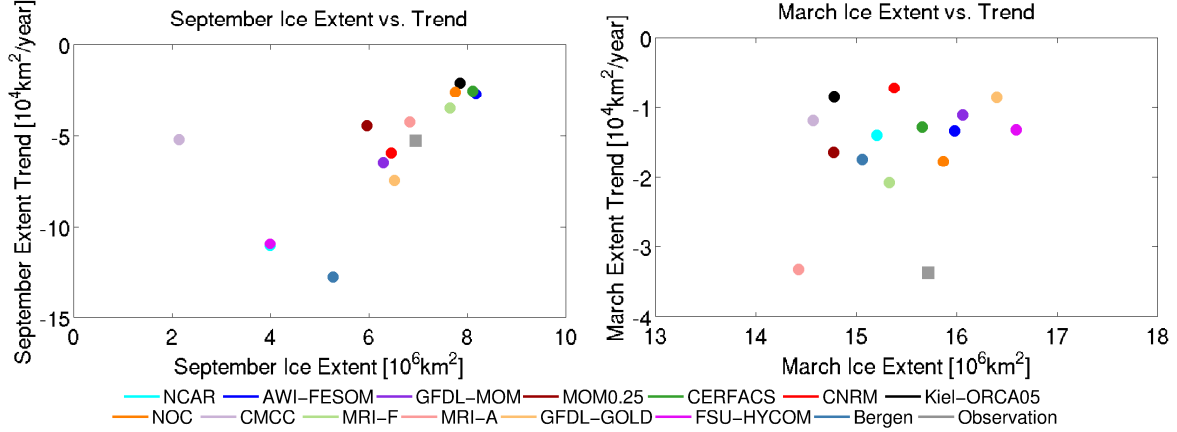


Figure 3: Northern Hemisphere (NH) sea ice extent [ $10^6\text{km}^2$ ] versus its trend [ $10^4\text{km}^2/\text{year}$ ]. Observations are shown with gray squares. Years 1979 - 2003 are used in the calculation. Note that the y-axis scales are different in the two panels.

the models with lower sea ice extent tend to have stronger interannual variability; the four models with extremely low sea ice extent have the strongest variability as also shown in Figure 2 (NCAR, CMCC, FSU-HYCOM, Bergen). The correlation between observed and modelled sea ice extent is moderately high for September, ranging from 0.6 to 0.8, and it is also rather good for most of the models in March (except for FSU-HYCOM, MRI-A, MRI-F and NOC).

The NH sea ice extent has a descending trend in both September and March according to the satellite observation (Figure 2, Table 2). Because it accelerates in the last few years, it is not appropriate to define a linear trend for the whole period. For our purpose we choose to evaluate the simulated linear trend for the period 1979 - 2003; and then the sea ice extent in 2007, the year when a low sea ice extent event was observed, will be compared.

All the models show downward trends for both the September and March sea ice extent, consistent to the observation (Table 2). The sea ice extent drops faster in September than in March, which is reproduced by the models. However, the spread in the simulated trend is large, particularly in September. NCAR, FSU-HYCOM and Bergen exhibit descending trends more than twice the observed one in September. They are among those that significantly underestimate the September sea ice extent. Kiel-ORCA05, CERFACS, NOC and AWI-FESOM have less than half of the observed descending trend in September. They are among the models that overestimate the sea ice extent. Therefore, the descending trend in sea ice extent roughly anti-correlates with the sea ice extent in September: models that overestimate the sea ice extent, tend to underestimate the descending trend, and vice versa (see Figure 3). The relationship between September sea ice extent and its trend can be explained by the fact that both of them can be influenced by sea ice thickness (see discussion in Section 3.1.2). The CMCC result is an exception in that it has very low sea ice extent for the whole integration period and has a low descending trend.

The descending trend of sea ice extent in March is underestimated in all the models except for MRI-A (Figure 3). The ensemble mean sea ice extent in March is lower than the observation in the 1980s, although it is very close to the observation afterwards (Figure 2, Table 2). This causes the simulated mean trend in March to be only about one third of the observed trend for the period 1979 - 2003. Therefore, in order to improve the representation of March sea ice extent trend, the winter sea ice extent in the colder years (the 1980s) needs to be tuned higher in terms of the model ensemble mean. Also because the model ensemble mean better represented the observed March sea ice extent in more recent years, the trend calculated using the whole period (1979 - 2007) compares with the observation better than considering the shorter period (Table 2).

A pronounced September sea ice extent minimum was observed in 2007 (Stroeve et al., 2008). Six models produced larger September sea ice extent than the observation in this year (AWI-FESOM, CERFACS, Kiel-ORCA05, NOC, MRI-F and MRI-A), and the aforementioned four models with low September sea ice extent in the whole period of the last decade have significantly lower value also in this year

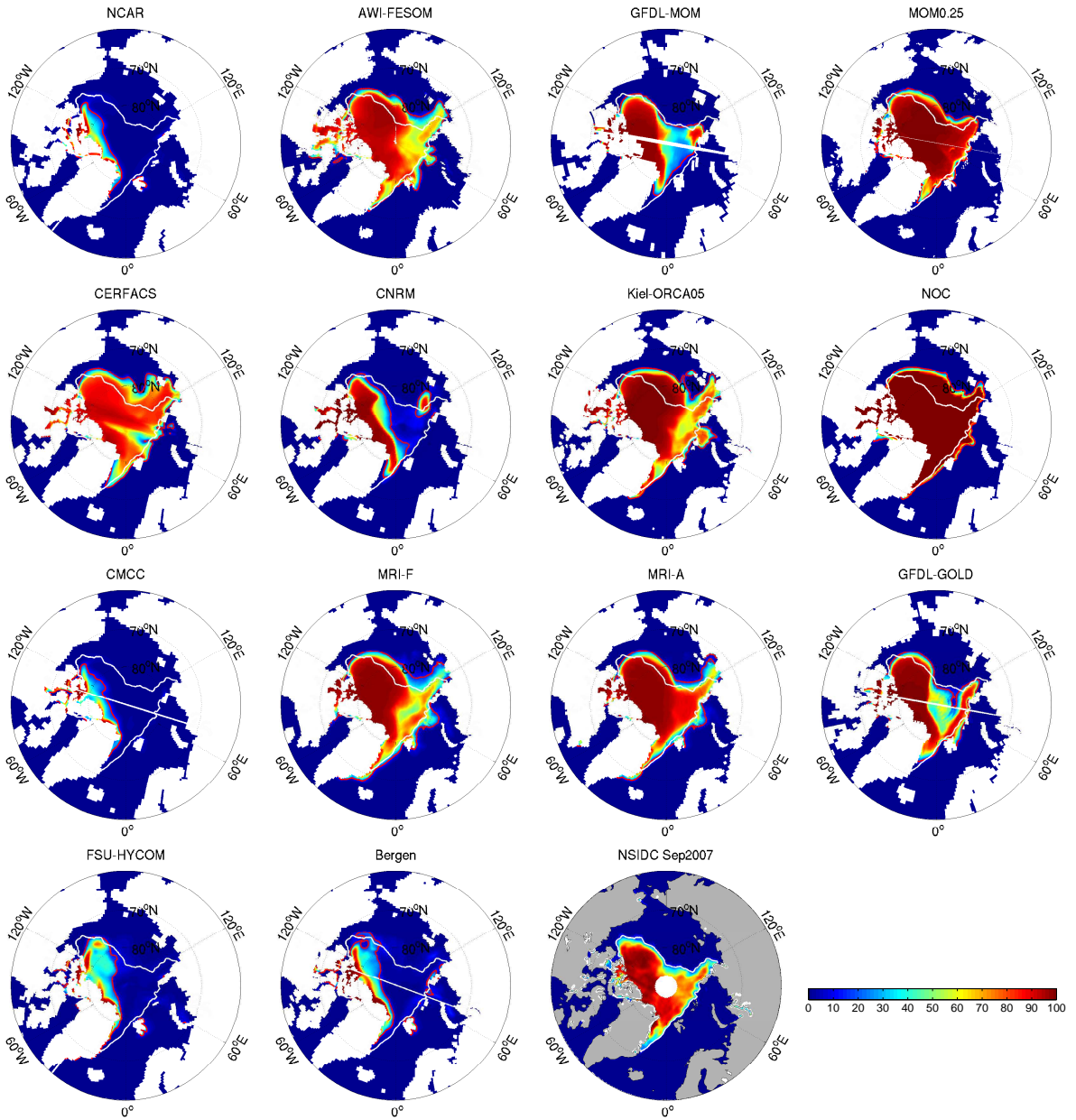


Figure 4: Observed and simulated sea ice concentration [%] for September 2007. The last panel is the satellite observation from NSIDC (Fetterer et al., 2002). The NSIDC 15% ice concentration contour line is shown in white; The simulated 15% ice concentration contour line is shown in red.

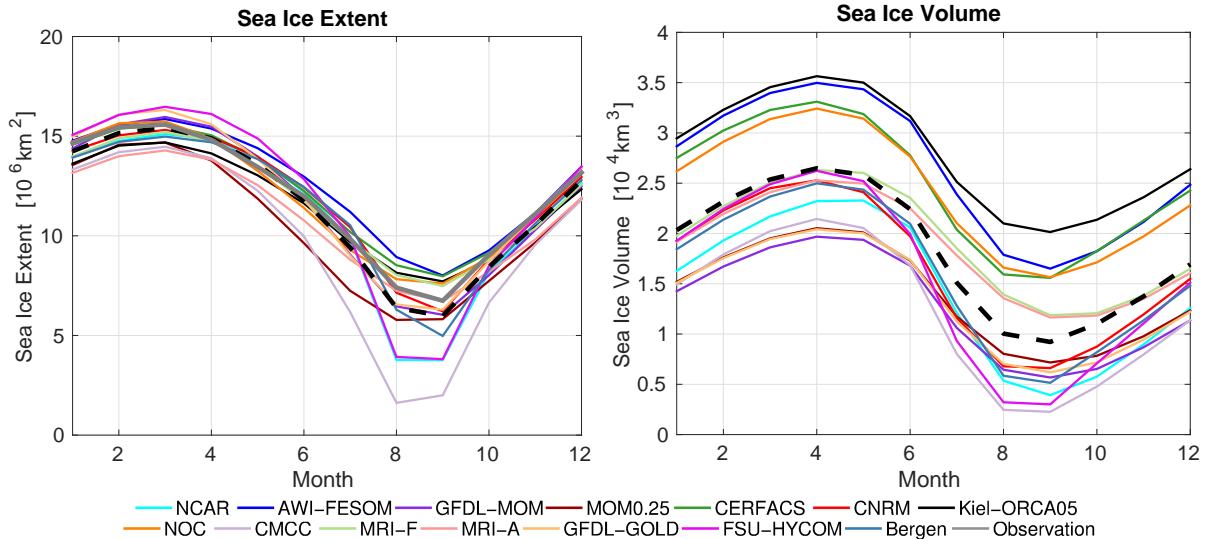


Figure 5: Seasonal cycle of Northern Hemisphere (left) sea ice extent [ $10^6 \text{ km}^2$ ] and (right) sea ice volume [ $10^4 \text{ km}^3$ ] averaged over the years 1979 - 2007. The model ensemble means are shown with dashed lines. The gray line in the left panel shows the observed sea ice extent (Fetterer et al., 2002).

(Table 2). The 2D distribution of sea ice concentration in September 2007 is compared to the observation in Figure 4. Five models have sea ice only along the northern boundary of the CAA, missing the observed sea ice at the North Pole and the ice tongue towards the Laptev Sea. In the other nine models, the observed sea ice retreat toward the North Pole from the Siberian side is reproduced, but most of these models show a weaker decline. GFDL-MOM and GFDL-GOLD have ice edges close to the observation in the western Arctic, but they have too low ice concentration near the North Pole. On the contrary, MOM0.25 and NOC have too high sea ice concentration. All the models tend to have more summer sea ice in the southern CAA than the observation. It was found that the downward shortwave radiation in the CORE normal year forcing has a negative bias, which can lead to overestimation of summer sea ice in the CAA (Wang et al., 2012). It is not clear if a similar bias exists in the CORE interannual forcing.

All the models have maximal sea ice extent in March, and nine models have the minimum in September, in agreement with observations (left panel of Figure 5). CMCC, NCAR, FSU-HYCOM and MOM0.25 have similar or even smaller sea ice extent in August than in September, different from the observed seasonality. The model spread in winter can be partly attributed to the difference in model ocean area, for example, in the CAA region, which is very differently represented by the models.

### 2.3. Sea ice extent in Barents Sea

The Barents Sea connects the Nordic Seas and the Arctic Ocean, and it is one of the two major pathways for Atlantic Water to enter the Arctic Ocean. Most of the oceanic heat that passes the Barents Sea Opening (BSO) is released to the atmosphere within the Barents Sea, so it is the most active region of air-sea heat exchange in the Arctic Ocean (Smedsrud et al., 2013). Sea ice extent in the Barents Sea has large interannual variability and it has a descending trend in recent years as shown by observations (Arthun et al. (2012), see Figure 6(left)). The most significant Arctic sea ice retreat is found in Barents Sea in simulations of future climate (Koenigk et al., 2013). Therefore, it is interesting to see how well sea ice in the Barents Sea is represented in the models.

All the models well reproduced the observed sea ice extent variability in the Barents Sea as shown by the anomaly of annual mean sea ice extent (Figure 6(left)).<sup>5</sup> The simulated sea ice extent is anti-correlated with the heat transport (referenced to  $0^\circ\text{C}$ ) through the BSO in all the models, with heat transport leading 0-1 year (Table 3). This supports the idea that the heat transport through the BSO drives the interannual variability of Barents Sea sea ice extent suggested by Arthun et al. (2012). The

<sup>5</sup>The anomaly is calculated by removing the temporal mean from the time series. The same for the anomalies in other figures.

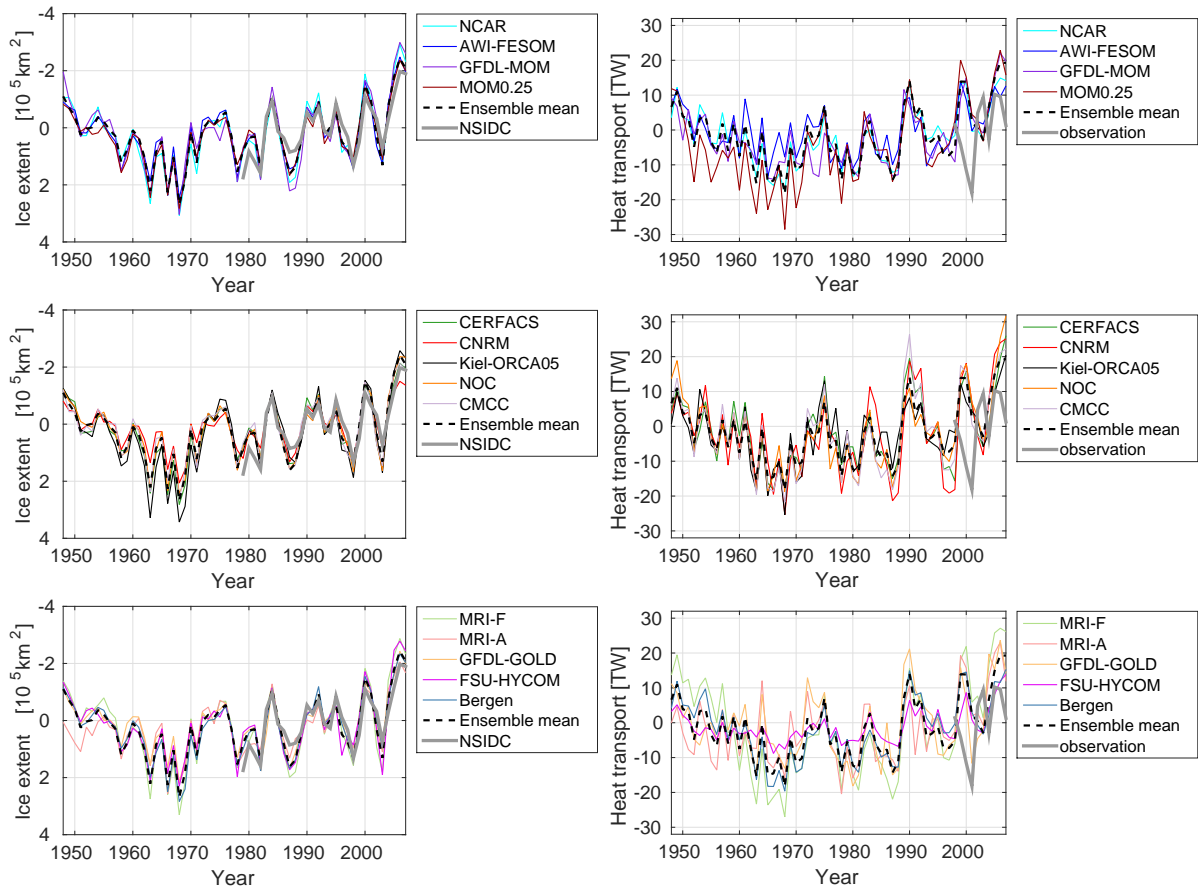


Figure 6: Anomaly of annual mean (left) Barents Sea sea ice extent and (right) BSO heat transport (referenced to  $0^\circ\text{C}$ ) in the last model loop. Observational data (Fetterer et al. (2002) and Smedsrud et al. (2013)) are shown with thick gray lines. Note that the vertical axes of sea ice extent are inverted.

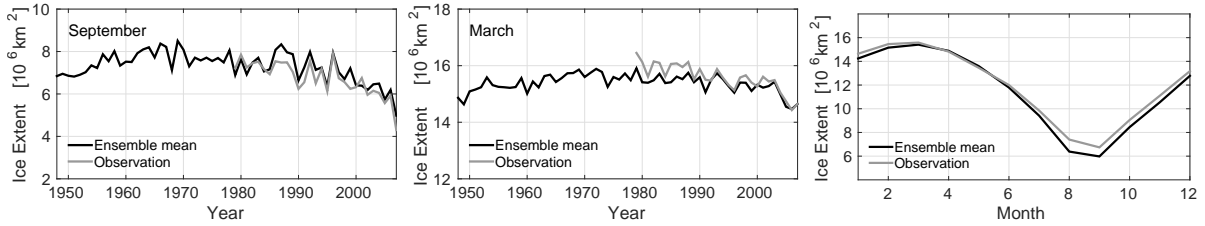


Figure 7: Model ensemble mean of the Northern Hemisphere sea ice extent for (left) September, (middle) March, and (right) the mean seasonal cycle. The observations from NSIDC are shown with gray curves.

interannual variability of BSO heat transport agrees well among the models, but the discrepancy to the observed heat flux is surprisingly high (Figure 6(right)). As shown by Arthun et al. (2012), the low spatial resolution of moorings can potentially produce large uncertainty in the observed heat flux, which might explain the difference between the observation and models.

Although the variability of sea ice extent in the Barents Sea is well reproduced, most of the models did not adequately simulate the mean values (Table 3). The bias of simulated mean sea ice extent cannot simply be explained by the simulated BSO heat transport: the highest heat flux is in MOM0.25, while the lowest sea ice extent is in CNRM. Overall, the interannual variation of the Barents Sea sea ice extent, including the magnitude of the variability, is a robust feature that is well represented in all the models, despite the spread in the simulated mean sea ice extent and mean heat transport.

Table 3: The Barents Sea sea ice extent, BSO heat transport, correlation coefficients between the annual mean Barents Sea sea ice extent and BSO heat transport at both 0 and 1 (heat fluxes lead) year lag. Positive heat transport indicates flux into the Barents Sea. The last 30 model years (1978 - 2007) are used in the analysis.<sup>1</sup>

	Observation	NCAR	AWI	MOM	MOM0.25	CERFACS	CNRM	Kiel	NOC	CMCC	MRI-F	MRI-A	GOLD	FSU	Bergen	mean	spread
ice extent	3.6 <sup>a</sup>	5.4	4.9	5.1	4.4	3.7	2.7	4.0	5.0	5.3	4.4	3.3	5.0	5.7	4.3	4.5	0.8
heat flux	70 ± 5 <sup>b</sup>	37.6	61.1	42.9	87.8	45.0	55.8	58.9	66.1	78.2	65.3	66.0	69.4	11.3	51.7	56.2	19.5
correlation 0		-0.77	-0.57	-0.74	-0.67	-0.80	-0.89	-0.61	-0.73	-0.72	-0.77	-0.68	-0.53	-0.85	-0.72	-0.72	0.10
correlation 1		-0.79	-0.71	-0.85	-0.70	-0.68	-0.82	-0.61	-0.69	-0.74	-0.74	-0.76	-0.74	-0.70	-0.74	-0.73	0.06

<sup>1</sup> Sea ice extent is shown in  $10^5 \text{ km}^2$ , and heat transport in TW. Heat transport is referenced to  $0^\circ\text{C}$ . All correlations are significant at the 95% confidence level. Observational data reference: (a) Fetterer et al. (2002), (b) Smedsrud et al. (2013). Missing values are shown with N/A, the same in other tables.

#### 2.4. Summary on the model ensemble mean of sea ice extent

In this section we summarize the simulated Northern Hemisphere (NH) sea ice extent based on the model ensemble mean. Other remarks will be given in the concluding section (Section 4).

- The mean sea ice extent in September is  $6.17 \times 10^6 \text{ km}^2$  averaged over the period of 1979 - 2003, smaller than the observation ( $6.95 \times 10^6 \text{ km}^2$ ) by about 11% (Table 2). The mean sea ice extent in March is closer to the observation than in September.
- In September the descending trend of NH sea ice extent is relatively well captured ( $-6.0 \times 10^4 \text{ km}^2/\text{year}$  compared to the observed trend of  $-5.3 \times 10^4 \text{ km}^2/\text{year}$  for the period of 1979-2003, Table 2). The models underestimate the sea ice retreat rate in March because they produce lower ice extent than the observation in the 1980s (Figure 7).
- Most of the observed high and low sea ice extent events are reproduced by the model ensemble mean (Figure 7). The mean correlation coefficients for the simulated and observed ice extent are 0.69 and 0.61 for September and March, respectively.
- The seasonal cycle of NH sea ice extent is well represented by the model ensemble mean. The models on average tend to have a stronger seasonal cycle with lower sea ice extent than the observation in summer.

### 3. Solid freshwater

Freshwater (FW) in the Arctic Ocean exists in the solid form mainly as sea ice and in the liquid form mainly located in the upper ocean. We discuss the modelled solid FW budget in this paper, and the liquid FW is present in another CORE-II Arctic paper (Wang and et al., 2015).

Arctic sea ice is mainly formed inside the Arctic Ocean, with a very small amount imported through Bering Strait (Woodgate and Aagaard, 2005). There is net sea ice export through the gateways at the Atlantic sector (Vinje et al., 1998; Kwok and Rothrock, 1999; Kwok et al., 2004; Kwok, 2007, 2009; Curry et al., 2014). The narrow CAA passages on the western side of Greenland impede sea ice flow and limit sea ice export from the Arctic Ocean, and the Fram Strait on the eastern side of Greenland is the main gateway for sea ice to leave the Arctic Ocean. High sea ice export through Fram Strait can cause noticeable negative salinity anomalies in the subpolar North Atlantic, called “Great Salinity Anomalies” (GSAs), thus impacting on deep water formation and the meridional overturning circulation (Dickson et al., 1988; Hakkinen, 2002). Sea ice volume continues to decline together with the retreat of both sea ice extent and thickness in the period of satellite observations (e.g., Kwok and Rothrock, 2009; Cavalieri and Parkinson, 2012; Comiso, 2012; Stroeve et al., 2012a; Laxon et al., 2013). It is crucial for numerical models to adequately represent the state and changes of sea ice in order to properly incorporate its roles in the climate system.

In the following we evaluate the simulated Arctic solid FW in the CORE-II models, with focus on the solid FW source terms and the solid freshwater content (FWC). Their mean state, interannual changes and seasonal variability are discussed in Sections 3.1, 3.2 and 3.3, respectively. A summary on the model ensemble mean of solid FW budget is given in Section 3.4.

#### 3.1. Mean state

##### 3.1.1. Solid freshwater sources

In this section we assess the mean state of the source terms for the Arctic solid FW, that is, the solid FW fluxes through the Arctic gateways and the sea ice thermodynamic growth rate. Table 4 shows the mean values of these diagnostics. In all the models solid FW fluxes through the gateways are the largest at Fram Strait. However, the solid FW fluxes have a big range among the models. At Fram Strait, the spread in the simulated solid FW flux is  $810\text{km}^3/\text{year}$ , about one third of the synthesized mean value ( $-2300 \pm 340\text{km}^3/\text{year}$ , Serreze et al. (2006)). Four models obtained Fram Strait solid FW fluxes within the uncertainty range of the synthesized value, including CERFACS, NOC, MRI-A and Bergen. Solid FW transport contains contributions from both sea ice and snow fluxes. It is found that the Fram Strait sea ice and snow fluxes are well correlated in terms of interannual variability, and that sea ice flux is the major contributor to the mean solid FW transport (accounting for more than 90% on average).

Table 4: Arctic Ocean solid freshwater (FW) source terms and solid freshwater content (FWC) relative to salinity 34.8. The last 30 years (1978 - 2007) are used in the analysis.<sup>1</sup>

	Observations	NCAR	AWI	MOM	MOM0.25	CERFACS	CNRM	Kiel	NOC	CMCC	MRI-F	MRI-A	GOLD	FSU	Bergen	mean	spread
Fram Strait	$-2300 \pm 340$ <sup>a,b,2</sup>	-1565	-3867	-1244	-1226	-2340	-1578	-1218	-2500	-1892	-3168	-2442	-1213	-1452	-2207	-1959	833
Davis Strait	$-427$ to $-644$ <sup>c,3</sup>	-644	-743	-420	-531	-769	-572	-348	-1051	-869	-690	-494	-387	-486	-977	-653	224
Bering Strait	$100 \pm 70$ <sup>d</sup>	42	100	23	12	70	82	70	86	98	-27	-15	6	-126	140	44	69
BKN		-560	-407	N/A	N/A	-174	-41	-554	-36	-473	-522	-250	N/A	-312	-94	-317	215
BSO		-171	-424	-141	-211	-369	-164	-122	-478	-258	-418	-260	-36	-353	-311	-270	139
thermodynamic		N/A	4503	N/A	N/A	N/A	N/A	N/A	3233	2568	4001	2865	N/A	2010	2970	3214	917
Arctic Storage		1.05	1.66	0.81	0.94	1.79	1.13	1.89	1.68	0.83	1.20	1.20	0.79	1.03	1.03	1.22	0.38
NH Storage	$1$ <sup>a</sup> to $1.68$ <sup>4</sup>	1.20	1.96	0.94	1.03	1.90	1.26	1.98	1.83	0.96	1.45	1.36	1.01	1.21	1.16	1.38	0.39

<sup>1</sup> FW fluxes and the sea ice thermodynamic growth rate are shown in  $\text{km}^3/\text{year}$ , and the FWC is in  $10^4 \text{ km}^3$ . Positive values indicate FW sources for the Arctic Ocean, and negative values indicate FW sinks. For the definition of FW transport and FWC see the Appendix A. Observational data reference: (a) Serreze et al. (2006), (d) Woodgate and Aagaard (2005), (b) Vinje et al. (1998), (c) Kwok (2007).

<sup>2</sup> Based on the winter sea ice export at Fram Strait from 2003 to 2008 analyzed by Spreen et al. (2009). Haine et al. (2015) gave an estimate of  $-1900 \pm 280 \text{ km}^3/\text{year}$  for the solid FW flux at Fram Strait in the period 2000-2010, indicating a decline compared to the climatological value suggested by Serreze et al. (2006).

<sup>3</sup> The recent estimate of sea ice export at Davis Strait using Upward-Looking Sonar (ULS) and satellite data for the period 2004-2010 is  $-315 \pm 32 \text{ km}^3/\text{year}$  (Curry et al., 2014).

<sup>4</sup> The FW stored in sea ice was estimated based on an assumption of 2 m ice thickness by Serreze et al. (2006). This approximation of sea ice thickness is probably too low at least for the late 20th century. Laxon et al. (2003) report a mean winter ice thickness of 2.73 m south of  $81.5^\circ\text{N}$  for 1993-2001. If we assume 3 m mean ice thickness, an estimate close to the values given by Aagaard and Carmack (1989) and Rothrock et al. (1999), the FW storage in sea ice will be  $1.5 \times 10^4 \text{ km}^3$ . The sea ice FW storage based on the PIOMAS Arctic sea ice volume reanalysis (Schweiger et al., 2011) is about  $1.68 \times 10^4 \text{ km}^3$  averaged from 1979 to 2007 (assuming sea ice density of  $910 \text{ kg/m}^3$  and salinity of 4 psu).

Sea ice FW flux depends on both sea ice thickness and drift velocity (see Appendix A for the definition of sea ice FW flux). Kiel-ORCA05 is one of the models with the thickest sea ice, but it has very low Fram Strait solid FW export; The Bergen model has too thin sea ice compared to the observation, but its Fram Strait solid FW export is close to the observed value. This indicates that the fidelity of simulated sea ice flux does not reflect the model skills in representing sea ice thickness and velocity. We will assess the Arctic sea ice thickness in Section 3.1.2.

The observed net solid FW flux at Davis Strait is toward the Labrador Sea (Kwok, 2007; Curry et al., 2014), and this direction is reproduced in all the models (Table 4). The largest export flux is in NOC and Bergen, with about twice the observed value. A small amount of solid FW is imported to the Arctic Ocean through Bering Strait according to observations (Woodgate and Aagaard, 2005), but three models obtained (small) export fluxes, including MRI-F, MRI-A and Bergen.<sup>6</sup>

The models agree that Arctic sea ice is exported at the BKN when averaged over the last 30 years, and the Barents Sea has net sea ice export through the BSO. In some models the amount of solid FW flux entering Barents/Kara Seas from the north is very similar to that leaving at the BSO, while some models have distinguishable difference between the two fluxes. NCAR, CERFACS, CNRM and Kiel-ORCA05 have larger fluxes at the BKN, but NOC and Bergen have larger outflow at the BSO. This means that there is no agreement in the models on whether the Barents/Kara Seas are a region of sink or source for sea ice.

The Arctic sea ice thermodynamic growth rate is provided by a few model groups. From these data we can conclude that the spread in sea ice production in the Arctic Ocean is the largest in the solid FW source terms (Table 4).

### 3.1.2. Solid freshwater content

Sea ice volume, thus the freshwater stored in sea ice, depends on the sea ice thickness. Before discussing the sea ice volume, we first evaluate the modelled sea ice thickness by comparing with observations. Sea ice thickness observations from submarines, moorings, field measurements and satellites are not continuous and very limited in space and time. The sea ice thickness fields derived from the ICESat satellite are available for a few months in spring and fall each year starting from 2003 (Kwok et al., 2009). For the purpose of model evaluation, we calculated the mean values for spring (Feb., Mar. and April) 2004-2007 for each model, and defined the observational field by averaging all available ICESat data in spring 2004-2007 (Figure 8).

The observed sea ice has larger thickness towards the CAA, and smaller thickness towards the Siberian coast. All models can reproduce this feature, but the simulated sea ice thickness differs from the observation significantly. This is also seen in the AOMIP models (Jahn et al., 2012a). The sea ice thickness along the northern coast of CAA is best simulated by AWI-FESOM and Kiel-ORCA, but they tend to have thicker sea ice than the observation towards the Siberian coast. CERFACS, NOC, MRI-F and MRI-A underestimate the sea ice thickness towards the CAA and overestimate the sea ice thickness towards the Siberian coast. Other models underestimate the sea ice thickness in most of the regions where satellite observations are available.

The five models which have too high September sea ice extent with low descending trend (AWI-FESOM, CERFACS, Kiel-ORCA05, NOC and MRI-F, see Figure 3), overestimate sea ice thickness in spring for the considered period (Figure 8). The three models with too low September sea ice extent and high descending trend (NCAR, FSU-HYCOM and Bergen), underestimate sea ice thickness. If the simulated sea ice in late winter and spring is too thick, more heat is needed to melt it to produce open ocean area in the melting season. Therefore, overestimated sea ice thickness could lead to too high sea ice extent in summer and underestimation of its trend. However, a few models with similar spring sea ice thickness turned out to have very different September sea ice extent, so model details need to be carefully examined in order to understand individual model behaviour and to improve sea ice thickness, concentration and their trend simultaneously.

After comparing the sea ice thickness, we focus on the sea ice FW storage in the following. The models show a spread of  $0.41 \times 10^4 \text{ km}^3$  in the sea ice FWC, about one third of the model mean value (Table 4). Due to lacking long term sea ice thickness observations, there are only rough estimates for the solid FWC in literature. Serreze et al. (2006) give an estimate of  $10^4 \text{ km}^3$  by assuming 2 m sea ice thickness. If we assume 3 m mean ice thickness, a value more representative for the sea ice state in the past few decades (Aagaard and Carmack, 1989; Rothrock et al., 1999), the FWC is  $1.5 \times 10^4 \text{ km}^3$ . The FW stored in sea ice based on the PIOMAS Arctic sea ice volume reanalysis (Schweiger et al., 2011) is about  $1.68 \times 10^4 \text{ km}^3$  averaged from 1979 to 2007 (assuming sea ice density of  $910 \text{ kg/m}^3$  and salinity of

---

<sup>6</sup> The sea ice transport at Bering Strait is very small compared to other Arctic gateways, so the model bias at this gateway has small impact on the total Arctic FW budget. In this paper we show the results for all major Arctic gateways for completeness. Quantifying impacts of model biases and their significance is not pursued.

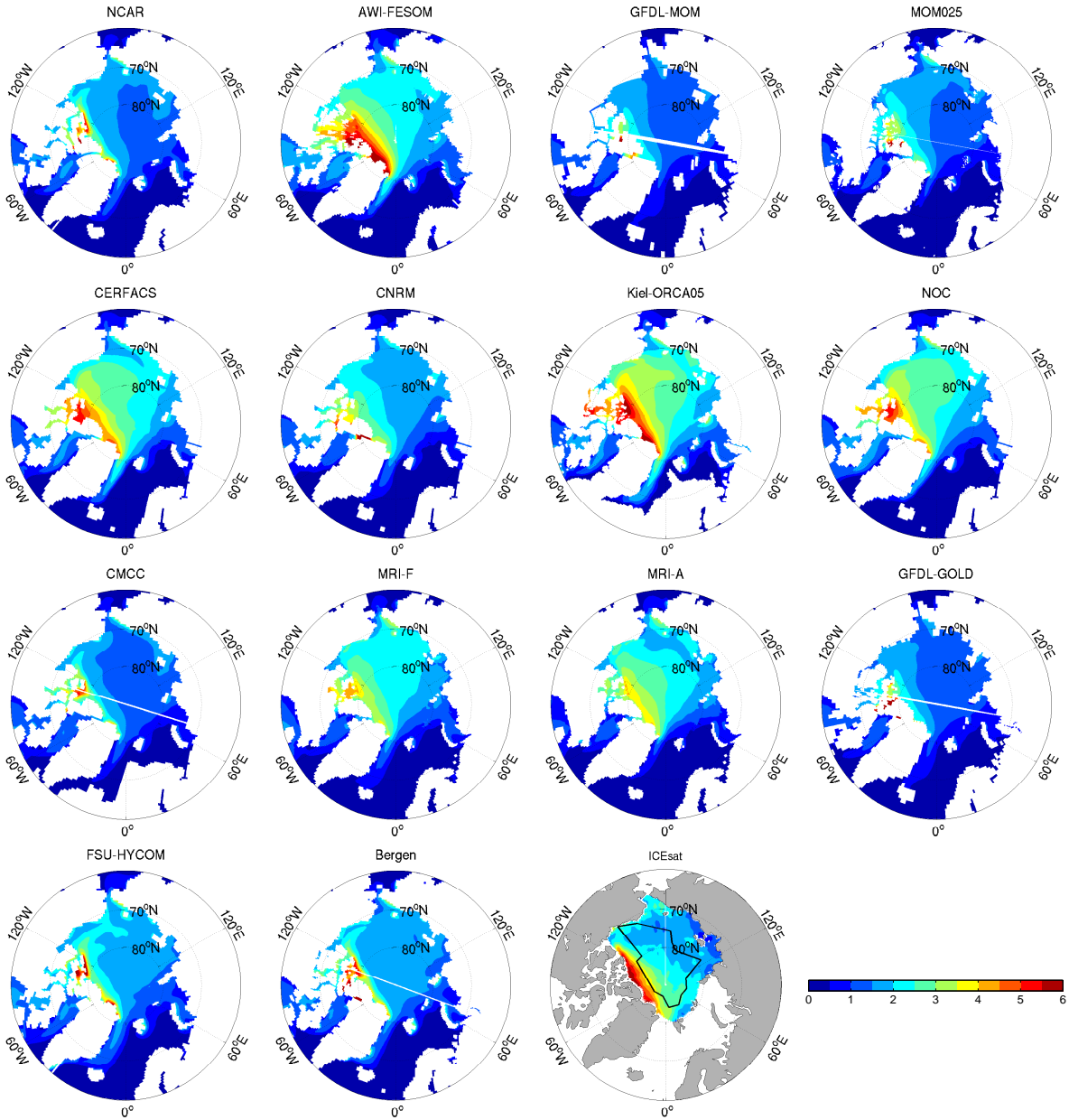


Figure 8: Observed and simulated spring sea ice thickness [m]. The last panel is the ICESat observation (Kwok et al., 2009). The model results are the mean values for spring (Feb., Mar. and April) 2004 - 2007 of the last model loop. The observation is the average over all available ICESat data in spring 2004 - 2007. The black polygon in the last panel indicates the region of the SCICEX box.

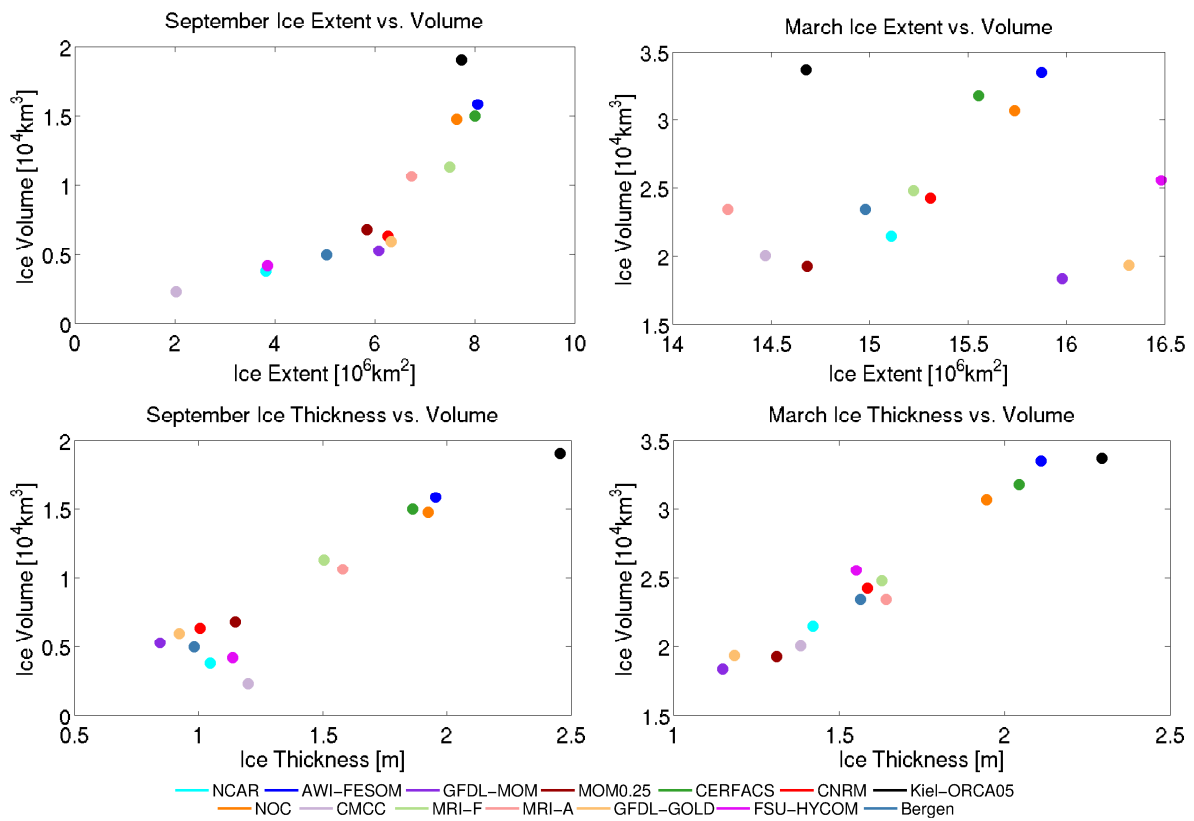


Figure 9: (upper) The relationship between Arctic sea ice volume [ $10^4 \text{ km}^3$ ] and extent [ $10^6 \text{ km}^2$ ]. (lower) The relationship between Arctic sea ice volume and thickness [m]. The last 30 model years (1978 - 2007) are used in the analysis.

4 ppt). The model ensemble mean of the NH solid FWC is  $1.37 \times 10^4 \text{ km}^3$ , within the range of different estimates mentioned above.

410 The model spread in sea ice volume can be attributed to the spread in sea ice thickness and extent. In September, the sea ice volume tends to be higher in models with larger sea ice extent, and vice versa, but this relationship is not found in March (Figure 9). The growth of Arctic sea ice extent is constrained by the surrounding continents when thickness and volume still increase in the freezing season. This can explain the weaker connection between sea ice extent and volume in March. Models with large ice  
415 volume tend to have thick sea ice in both September and March. Although the sea ice volume correlates with sea ice extent in September, the spread in sea ice volume is mainly caused by the difference in sea ice thickness (except for the four models with too low ice extent: CMCC, NCAR, FSU-HYCOM and Bergen). This is because the range of September sea ice extent among the models is about  $6-8 \times 10^6 \text{ km}^2$ , while the highest sea ice thickness is about 3 times the lowest (0.8 – 2.4 m). The four models that have  
420 largest sea ice volume (Kiel-ORCA05, CERFACS, NOC and AWI-FESOM, see Table 4) have thicker sea ice than the other models (Figure 8).

### 3.2. Interannual Variability and trend

In this section we first discuss the statistics of the annual mean solid FW budget. Then the interannual variability of solid FW transport through each Arctic gateway is examined in Section 3.2.1. The variation  
425 of solid FWC in the Arctic Ocean is analyzed in Section 3.2.2, where the focus is on (a) the relationship between sea ice volume and thickness and (b) the sources of sea ice volume changes.

Table 5: Standard deviation of the Arctic Ocean solid freshwater (FW) fluxes and solid freshwater content (FWC) for the last 30 model years (1978 - 2007). It is calculated using annual mean time series.<sup>1</sup>

	Observations	NCAR	AWI	MOM	MOM0.25	CERFACS	CNRM	Kiel	NOC	CMCC	MRI-F	MRI-A	GOLD	FSU	Bergen	mean	spread
Fram Strait	401 <sup>a</sup> to 774 <sup>b,2</sup>	312	574	246	275	429	295	295	511	333	596	580	229	231	453	367	130
Davis Strait		34	147	78	119	162	94	80	174	172	119	108	71	84	169	124	39
Bering Strait		51	97	20	52	46	47	39	92	62	112	103	10	61	65	58	29
BKN		302	588	N/A	N/A	969	621	345	660	365	662	533	N/A	369	550	462	144
BSO		126	183	85	107	225	91	88	241	144	198	152	29	164	205	148	66
thermodynamic		N/A	1170	N/A	N/A	N/A	N/A	N/A	1066	799	884	907	N/A	725	902	924	166
Arctic Storage		N/A	0.15	0.10	0.11	0.19	0.11	0.22	0.18	0.07	0.12	0.11	0.09	0.08	0.11	0.13	0.05
NH Storage		0.10	0.19	0.11	0.12	0.22	0.13	0.23	0.20	0.09	0.14	0.12	0.11	0.10	0.13	0.14	0.05

<sup>1</sup> The standard deviation of FW fluxes is in  $\text{km}^3/\text{year}$ , and FWC is in  $10^4 \text{ km}^3$ . Observational data reference: (a) Kwok et al. (2004), (b) Vinje et al. (1998).

<sup>2</sup> Calculated from the annual mean data provided in the work of Kwok et al. (2004) and Vinje et al. (1998). Sea ice density of  $910 \text{ kg/m}^3$  and salinity of 4 psu are used in the calculation.

We define the strength of interannual variability using the standard deviation of the annual mean time series. The models agree that the sea ice thermodynamic growth rate has the strongest interannual variation among the solid FW source terms (see Table 5, and note that the thermodynamic growth rate  
430 data are available from seven models). The strongest interannual variation in lateral solid FW fluxes happens at the Fram Strait and BKN. Sea ice drift changes direction in the region of Barents/Kara Seas depending on the changes in sea level pressure patterns in that region (Kwok et al., 2005), which can lead to changes in the distribution of sea ice export through the two close gateways, thus enhancing the variability. Most models have similar variability strength at these two gateways except for CERFACS  
435 and CNRM, which have much stronger variation at the BKN. The standard deviation of the observed 5-8 years time series of sea ice export at Fram Strait is  $401 - 774 \text{ km}^3/\text{year}$  (based on the data provided by Vinje et al., 1998; Kwok and Rothrock, 1999; Kwok et al., 2004). The model results calculated from the 30 years time series tend to underestimate those observations (Table 5). However, when we calculate the modelled standard deviation over the period of the observations, the model results agree better with  
440 the observed values (not shown). At the Fram Strait and BSO, models with larger solid FW transport tend to have stronger variability; this rough relationship is not found at other gateways.

#### 3.2.1. Solid freshwater sources

The annual mean sea ice FW transports at Fram Strait in the period of available observations are shown in Figure 10. Although the magnitudes differ significantly among the models, their interannual variability agrees well with the observations. The observed high sea ice export in 1994-1995 is reproduced  
445 in all the models. The anomaly of annual mean solid FW fluxes for the last 60 model years are shown in Figure 11. In addition to the high export event in 1994-1995, all models also agree on a few other high export events at Fram Strait, among which the strongest export took place in 1968. The high sea ice export in 1968 caused strong negative salinity anomaly in the subpolar North Atlantic in later years, described as the “great salinity anomaly” (GSA) in the 1970s by Dickson et al. (1988).  
450

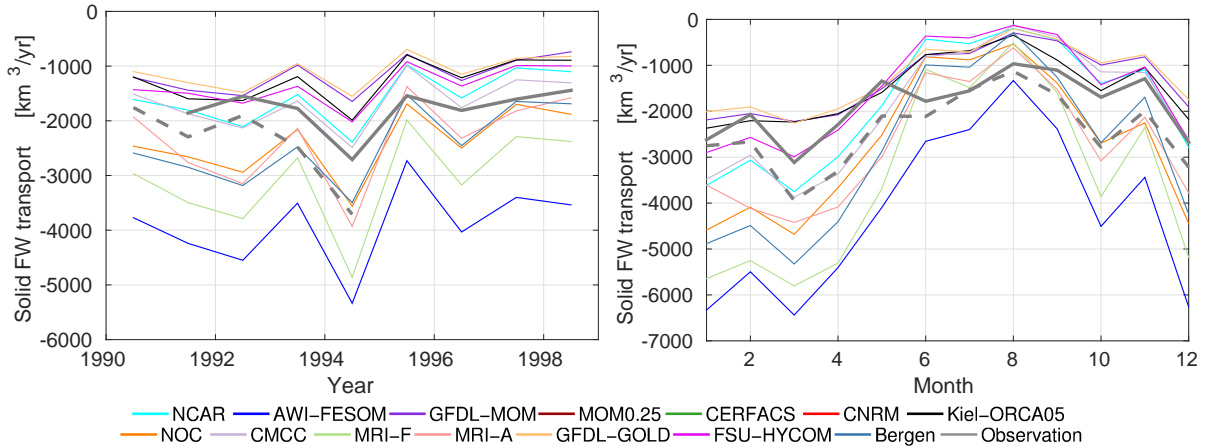


Figure 10: Fram Strait sea ice freshwater transport: (left) annual mean and (right) seasonal cycle. Observations are shown with gray thick lines: The solid lines are the estimate by Kwok and Rothrock (1999) and Kwok et al. (2004), and the dashed lines are the estimate from Vinje et al. (1998). In the left panel the winter-centered (from July to the next June) annual means are shown. A positive transport means a source for the Arctic Ocean.

Some of the models also show increased solid freshwater export at the BKN and BSO in 1968. At the BSO section, the solid freshwater export has relatively weak variability, with enhanced export standing out in 1968, although the magnitude of enhancement is quite different among the models. The wintertime sea ice drift velocity is predominantly oriented from the Barents/Kara Seas towards the Arctic basin in 1999/2000; sea ice drift changes direction towards the Barents Sea in 2002/2003 due to the changes in the location of the sea level pressure low (Kwok et al., 2005). Among the eleven models with BKN data available, eight models simulated net FW transport towards the Arctic basin at the BKN in 1999/2000 as suggested by observations (including NOC, Bergen, CERFACS, AWI-FESOM, MRI-A, MRI-F, CNRM and FSU-HYCOM, not shown), although all the models can get positive *anomaly* (Figure 11). All the models reproduced the transition from the positive anomaly in 1999/2000 to the negative anomaly in 2002/2003 as suggested by observations.

Recent observations show increasing sea ice export at Davis Strait from 2005 to 2007 (Curry et al., 2014)<sup>7</sup>, which is reproduced by all the models (Figure 11). For the longer period of the last 15 model years, the models have decreasing tendency in solid FW export through the Davis Strait. However, the changes throughout this period are similar to the magnitude of decadal variability, so we cannot define the tendency in this period as a persistent trend related to climate change without considering extra information.

The correlation of annual mean solid FW fluxes between models are very high at Fram, Davis, and Bering Straits and the BSO (not shown). The good correlation between the models conforms to the consensus that sea ice drift, predominately determined by wind forcing, has large impact on sea ice volume transport variability (e.g., Kwok and Rothrock, 1999; Dickson et al., 2000; Vinje, 2001).

Sea ice thickness can also contribute to the variability of sea ice volume export (Köberle and Gerdes, 2003; Haak et al., 2003; Koenigk et al., 2006). The large sea ice export event in 1968 was preceded by a positive sea ice thickness anomaly in the Laptev Sea region in 1965/1966, which propagates towards the Canadian sector and flushes out through the Fram Strait in 1968 (Haak et al., 2003). Most of the CORE-II models show a Fram Strait sea ice thickness maximum in 1968 except for NCAR, CMCC, FSU-HYCOM and Bergen, which have highest sea ice thickness at Fram Strait in 1965 (not shown). These four models have too low sea ice thickness and summer ice extent compared to observations (Figures 2 and 8). The interpretation of the role played by Arctic sea ice thickness in these models is not robust, even though they also obtained high sea ice volume export in 1968. When we want to quantify the relative contribution of accumulated sea ice in the Arctic Ocean compared to the direct effect of enhanced sea

<sup>7</sup>Note that sea ice transport decreased again in 2009 and 2010 in the observation, which is beyond the period of model simulations.

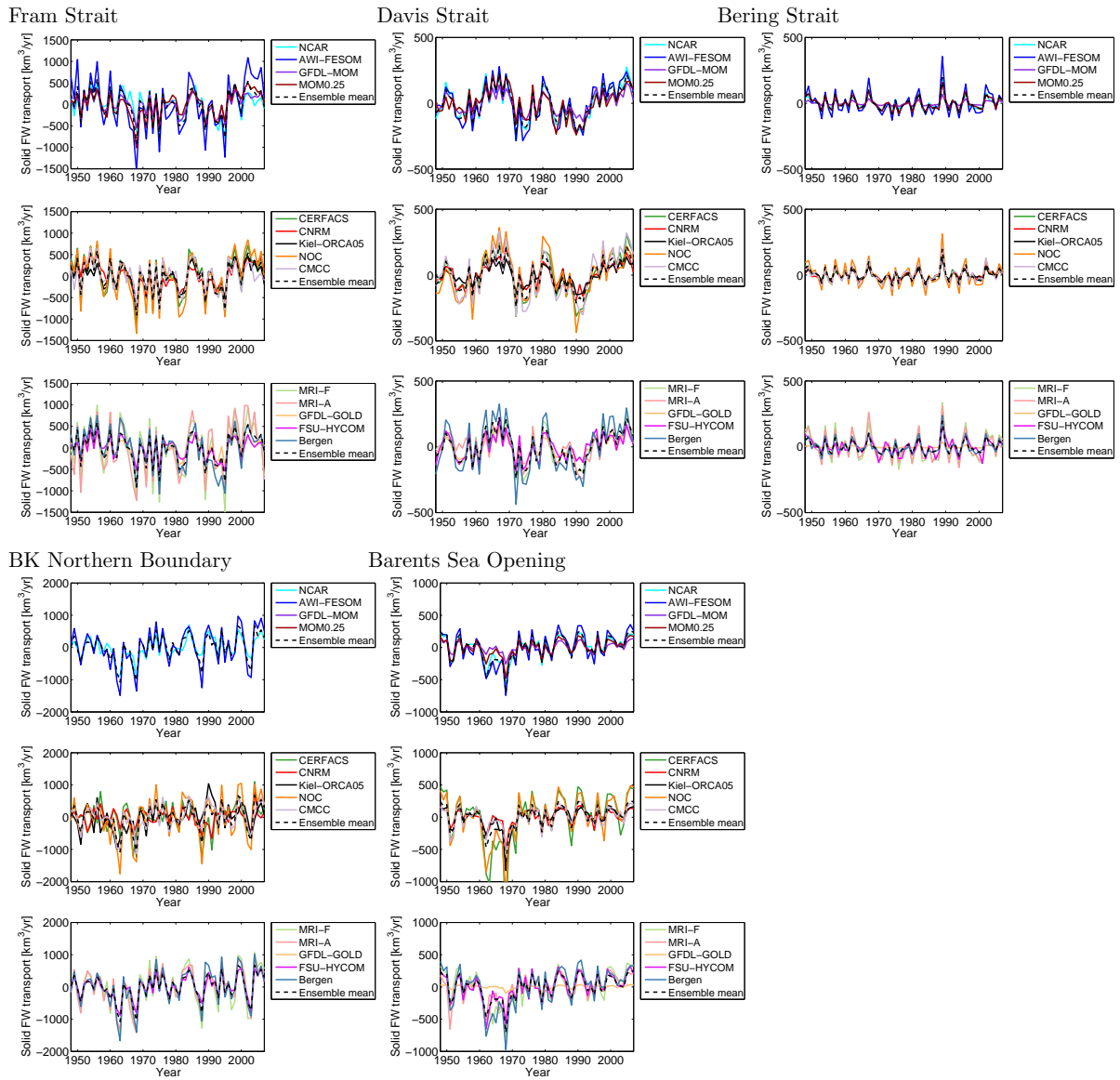


Figure 11: Anomaly of the annual mean solid freshwater transport through the Arctic gateways in the last model loop. Positive transport means a source for the Arctic Ocean.

ice drift, the models need to faithfully simulate the sea ice thickness.

No significantly high correlations between solid FW transports at different gateways are found when we consider the last 30 years or the whole 60 years. However, some pronounced events show correlation or anti-correlation between the Fram Strait and BKN sections, with agreement among the models. For example, when the BKN export increases from 1999/2000 to 2002/2003, the Fram Strait export decreases, which can be explained by the changes in sea ice drift velocity in the region of Barents/Kara Seas caused by changes in the location of local sea level pressure lows (Kwok et al., 2005). A different situation happened in 1968, when the Fram Strait and BKN have enhanced export fluxes simultaneously. The correlation between transports at the BKN and BSO is not significant (correlation coefficients less than 0.5 at 0-1 year lag, not shown), which can be explained by the importance of thermodynamic processes within Barents/Kara Seas.

### 3.2.2. Solid freshwater content

The Arctic annual mean sea ice volume in the period 1978 - 2007 has a descending trend in all models (Figure 12a). The increasing trend at the beginning of the model loop is caused by using the 2007 results of the proceeding loop as the initial condition. Models with larger descending trends in sea ice thickness (the spatial mean averaged where sea ice exists) tend to have larger descending trends in sea ice volume (Figure 12b). The four models with thickest sea ice (Kiel-ORCA05, CERFACS, NOC and AWI-FESOM) have largest trends in both sea ice thickness and volume. Trends in the Arctic sea ice volume and thickness seemingly can be used as equivalent diagnostics for quantifying sea ice response to climate change, but not the Arctic sea ice extent (compare Figures 12b,c).

The simulated trend of sea ice thickness can be evaluated using the observational data based on the long period of submarine tracks and recent satellite measurements. Rothrock et al. (2008) analyzed the historical submarine observations in a polygon in the Arctic Ocean, the so-called "SCICEX box" (see Figure 8 for the location) and provided spatial mean sea ice thickness estimates for the period 1975 - 2000. This dataset was extended by combining the ICESat measurements (Kwok and Rothrock, 2009). The observed and the simulated annual mean sea ice thickness in the SCICEX box is shown in Figure 13. The models tend to underestimate the mean thickness and the descending trend. The trend of the model ensemble mean for the period 1980 - 2007 is  $-8.2(\pm 1.3)\%$  per decade, about half of the observed trend of  $-16.5(\pm 7)\%$  per decade (Kwok et al., 2009). Although the CORE-II models underestimated the sea ice thinning trend, they obtained larger trend than CMIP climate models, which underestimated the observed trend by a factor of about 4 (Rampal et al., 2011). The satellite observation shows an accelerated thinning after 2003, which is not well captured by most of the CORE-II models.

The models agree with each other very well in the variability of sea ice volume (correlation coefficients between models after linear trends removed are larger than 0.7 for the last 30 model years, not shown). The events of large sea ice volume (e.g., mid of 1960s and end of 1980s) and the fast decrease following them are consistently simulated (Figure 12a). The interannual variability of sea ice volume can be better explained by that of sea ice thickness in most of the models (Figure 12d). The correlation between sea ice volume and sea ice thickness is relatively weak only in three models that have too low sea ice thickness and extent (NCAR, CMCC and FSU-HYCOM); Bergen has also very low sea ice thickness and extent, but its sea ice volume is well correlated with sea ice thickness as in most other models.

Changes in the Arctic sea ice volume can be induced by both the thermodynamic growth rate and lateral transport through the gateways. Sea ice volume decreases in the last 30 years because the total sink is larger than the total source (Table 4), while its interannual variability is caused by the variability of both terms. Their anomalies together with the time derivative of Arctic sea ice volume are shown in Figure 14. The models agree on the interannual variability for all three time series, but the strength of variability has a range among the models. The sea ice transport and thermodynamic growth rate are sometimes out of phase. When the strong sea ice export happened in 1968, sea ice production increases and partly compensates the sea ice reduction. They can be in phase sometimes, for example at the beginning of the 1980s, both terms are in favour of reducing Arctic sea ice volume (except for CMCC which does not produce enhanced sea ice export). Although there is no persistent trend in both thermodynamic growth rates and sea ice export when the period of last 30 model years is considered, they are in a low phase in the last decade.

To better compare the roles of two sea ice sources in the variation of sea ice volume on longer time scales, we calculated the anomaly of mean sea ice budget for two periods: 1986-1995 and 1995-2007 (Figure 15). These two periods are separated by events of large drop in sea ice volume (Figure 12). In

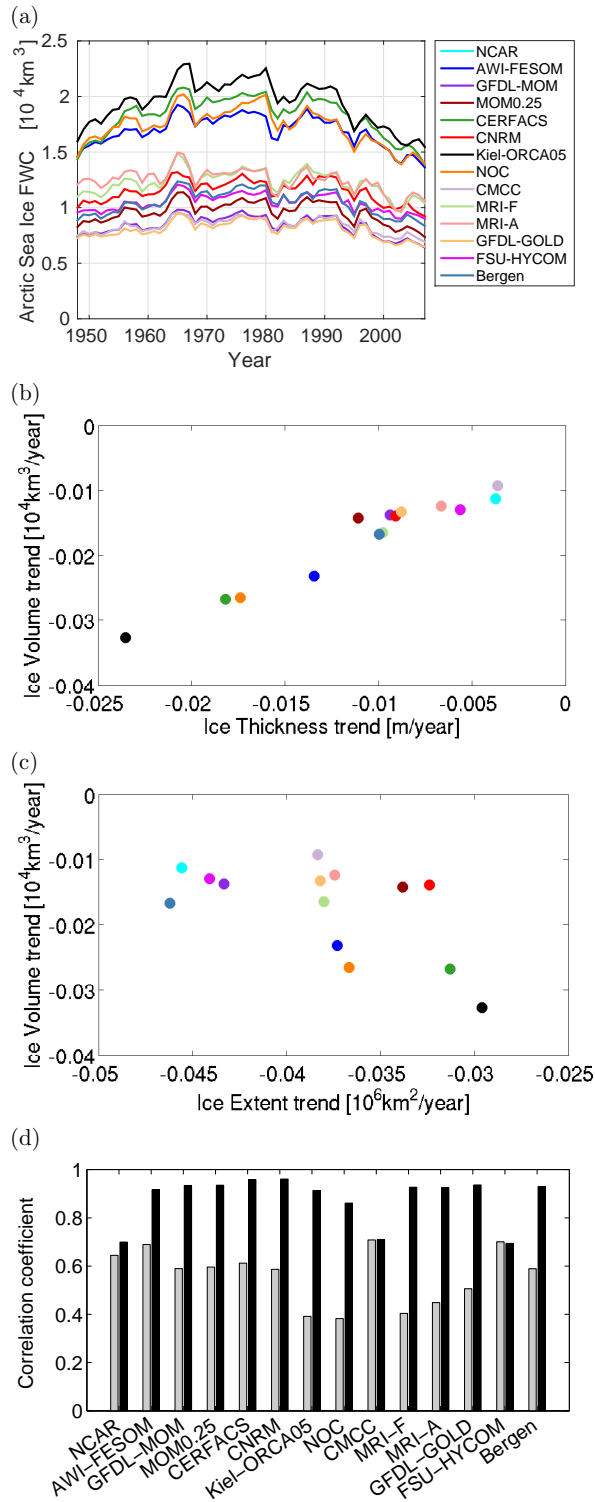


Figure 12: (a) Northern Hemisphere annual mean sea ice freshwater content [ $10^4 \text{ km}^3$ ] in the last model loop. (b) Linear trend of sea ice volume vs. that of thickness. (c) Linear trend of sea ice volume vs. that of extent. The legend for (c) and (d) is the same as in (a). (d) Correlation between sea ice volume and extent (gray), and between sea ice volume and thickness (black). The correlation coefficients are calculated using annual means after removing linear trends. The last 30 years (1978 - 2007) are used in the calculations for (b,c,d).

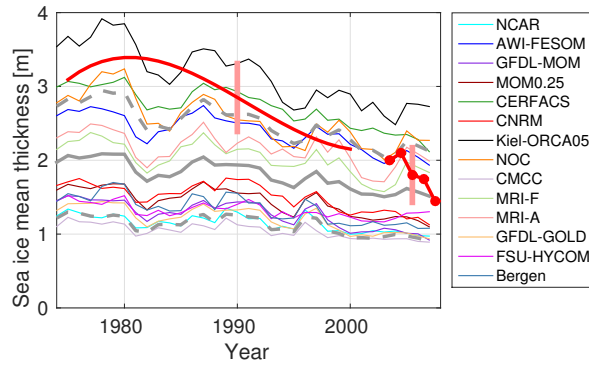


Figure 13: Simulated annual mean sea ice thickness in the SCICEX box compared with observations. The SCICEX box region is shown in the last panel of Figure 8. The model ensemble mean is shown with the thick gray line, with dashed gray lines showing plus/minus one standard deviation. The thick red solid line shows the annual mean estimate from submarine data (Rothrock et al., 2008), and the red line with circles shows ICESat data reported by Kwok and Rothrock (2009). Light red error bars show residuals in the regression of Rothrock et al. (2008) and the error estimate of ICESat data (Kwok and Rothrock, 2009).

the first period the sea ice production has positive anomaly while sea ice transport has negative anomaly. In the second phase both sources changed sign, so they still tend to compensate each other. The models agree that the two sources are out of phase on decadal time scales, and the magnitudes of the two sources are correlated in the models (one term is larger, then the other is also larger).

Note that splitting the sea ice volume sources as done above does not reveal separate roles of thermal forcing and wind forcing. Wind can affect both thermodynamic growth by opening and closing areas of open water, and sea ice export by changing sea ice drift, while air temperature can affect thermodynamic growth directly and ice export by changing sea ice thickness. Using sensitivity experiments Köberle and Gerdes (2003) showed that sea ice export is more closely linked to wind forcing and thermodynamic growth is somewhat more related to thermal forcing on the interannual time scale, but both forcing terms are important on long time scales. Good agreement on the simulated sea ice volume variability indicates that the models can relatively well represent the effect of different atmospheric forcing components.

### 3.3. Seasonal variability

In this section we assess the seasonality of the Arctic solid FW budget. Solid FW export occurs predominantly in wintertime at the Fram Strait, Davis Strait, BSO and BKN (Figure 16). Vanishing transports in summertime are associated with nearly ice-free conditions at Davis Strait, Bering Strait and the BSO. Four models (FSU-HYCOM, MRI-F, MRI-A and MOM0.25) simulate export transport in winter at Bering Strait, which is different from other models and observations (Woodgate and Aagaard, 2005). No linkage between model resolution and the magnitude and variability of solid FW transport at Bering Strait is found.

At the BKN, the models have low transport values in the summertime because the transect is close to the summer ice edge. Eight models agree on positive (towards the Arctic Ocean) transports in January. These models are those that produced correct ice flow direction in 1999/2000 (see Section 3.2.1). The seasonality is not found to be correlated with sea ice thickness, so the sea ice drift velocity mainly determines the seasonal changes in solid FW transport at the BKN section.

Fram Strait has the largest seasonal variation in solid FW transports among the five gateways. The models agree that the Fram Strait export is the weakest in August. The comparison to observations indicates that all models capture the seasonal changes, but tend to underestimate the export flux in summer and overestimate it in winter (Figure 10). The solid FW export in November is lower than in October in observations and most models in the 1990s (the period of available observations), but this is not seen in the mean seasonal cycle averaged over the last 30 years (cf. 10 and 16). This indicates that the details of the seasonal cycle vary on decadal time scales. The spread in winter transports is large among the models (ranging from about 2000 to 5000 km<sup>3</sup>/year). Kiel-ORCA05 has the largest sea ice thickness (Figure 9), but it has the weakest March export; the sea ice thickness of MRI-F is in the middle

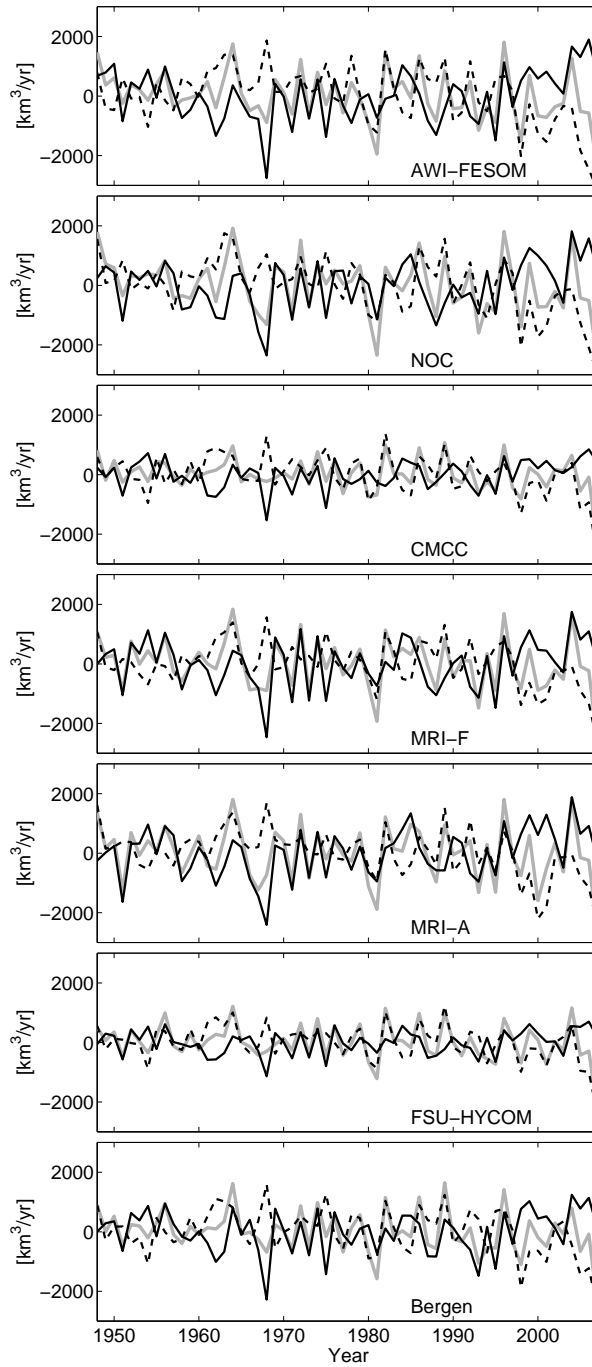


Figure 14: Anomaly of Arctic sea ice budget. The time derivative of sea ice volume is shown with gray lines; the net sea ice export flux is shown with solid black lines; and the net sea ice thermodynamic growth rate is shown with dashed black lines. Data are available from seven models. Positive values mean source for the Arctic Ocean.

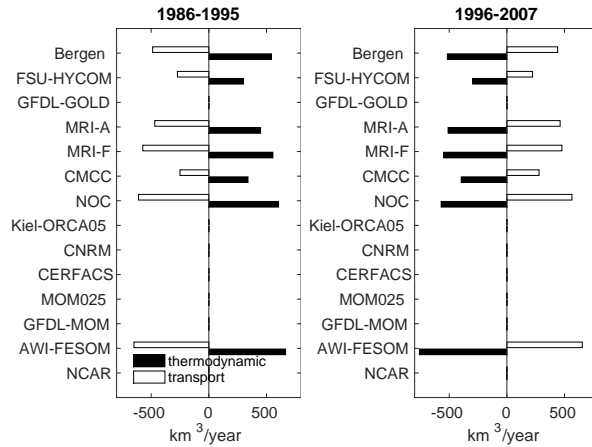


Figure 15: Sea ice sources [ $\text{km}^3/\text{year}$ ] averaged over two periods: (left) 1986-1995 and (right) 1995-2007. The anomaly from the last 30 years mean (1978 - 2007) is shown. Both the sea ice thermodynamic growth rate and transport through the gateways are defined such that positive values refer to sources for the Arctic Ocean. Therefore, negative transport anomaly means larger export than the mean value.

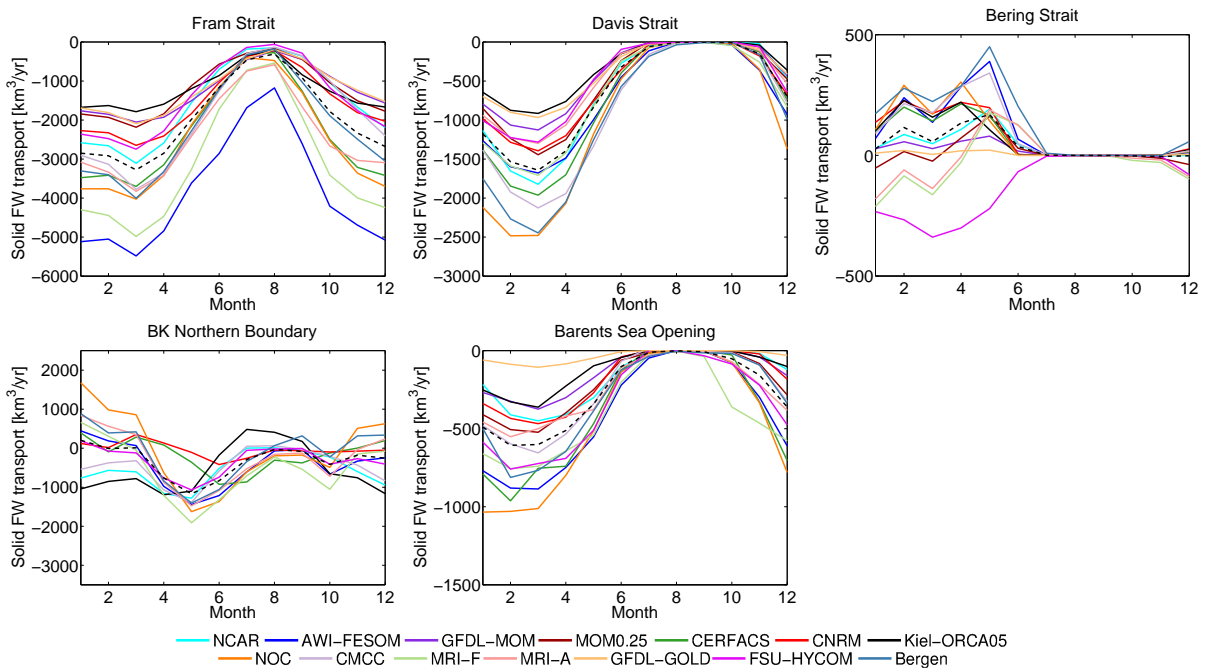


Figure 16: Mean seasonal cycle of solid freshwater transport through the Arctic gateways averaged over the last 30 years (1978 - 2007). The dashed lines show model ensemble means. Positive transport means source for the Arctic Ocean.

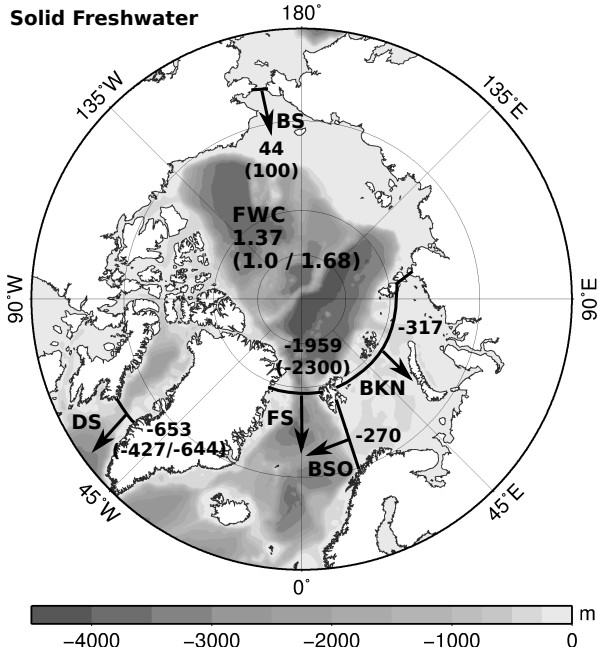


Figure 17: Model ensemble mean of solid freshwater budget of the Arctic Ocean. FW fluxes through the Arctic gateways are shown in  $\text{km}^3/\text{year}$ , and the FWC is in  $10^4 \text{ km}^3$ . The synthesized climatological values are shown in brackets; see Table 4 for their reference. The five main gateways are shown: Fram Strait (FS), Davis Strait (DS), Bering Strait (BS), Barents/Kara Seas northern boundary (BKN), and southern Barents Sea Opening (BSO). The last 30 model years (1978 - 2007) are used in the calculation.

of the spread, but it has the second strongest winter export. Therefore, the spread in the simulated solid FW export seasonality is caused by model spread in both sea ice thickness and drift velocity, which are dynamically linked to each other. Note that the uncertainty in observational estimates used in Figure 10 is also large. Although the same observed ice thickness profiles are used by Vinje et al. (1998) and Kwok and Rothrock (1999), they obtained ice flux estimates with differences of up to 30% because they used different ice drift estimates.

The seasonal variation of Arctic sea ice volume is mainly caused by the strong seasonal cycle of sea ice freezing and melting, not the lateral transport (not shown). The models agree on the seasonality of sea ice volume, with maximum in April and minimum in September, although the August (or October) sea ice volume is similar to their September values in a few models (Figure 5). The magnitude of seasonal variation (maximum minus minimum) is the smallest in MRI-A and largest in FSU-HYCOM, and the latter is about 70% higher than the former. No connection between the magnitude of seasonal variation and the mean sea ice volume is found.

### 3.4. Summary on the model ensemble mean of solid FW

In this section we summarize the simulated solid FW budget based on the model ensemble mean. Other general remarks are given in the concluding section (Section 4).

#### 1. Solid FW mean state

- The model ensemble mean represents the canonical scenario of the Arctic solid FW budget: The Arctic Ocean feeds solid FW to the subpolar North Atlantic mainly through Fram Strait, and receives a very small amount of sea ice through Bering Strait (Table 4, Figure 17). On average the models show small export fluxes at Davis Strait and the BKN.
- The simulated mean solid FW export through Fram Strait is  $-1959 \text{ km}^3/\text{year}$ , at the lower bound of the synthesized value ( $-2300 \pm 340 \text{ km}^3/\text{year}$ , Serreze et al., 2006; Vinje et al., 1998). The mean solid FW export through Davis Strait is  $-653 \text{ km}^3/\text{year}$ , comparable to the values suggested by observations ( $-427$  to  $-644 \text{ km}^3/\text{year}$ , Kwok, 2007).

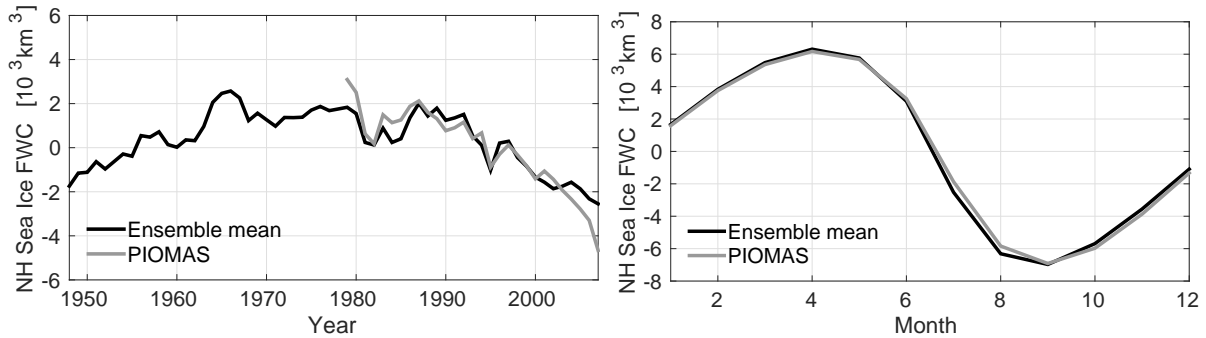


Figure 18: Anomaly of model ensemble mean of solid freshwater content (FWC) in the Arctic Ocean: (left) the annual mean time series and (right) the seasonal cycle. Sea ice FWC derived from PIOMAS Arctic sea ice volume reanalysis (Schweiger et al., 2011) is shown with gray curves; Sea ice density of  $910 \text{ kg/m}^3$  and salinity of 4 ppt are assumed.

- The synthesized value of FW stored in sea ice has large uncertainty because of lacking continuous observations of ice thickness. It is estimated to be  $10^4 \text{ km}^3$  using 2 m ice thickness by Serreze et al. (2006). The FW stored in sea ice based on the PIOMAS sea ice volume reanalysis (Schweiger et al., 2011) is about  $1.68 \times 10^4 \text{ km}^3$  averaged from 1979 to 2007 (assuming sea ice density of  $910 \text{ kg/m}^3$  and salinity of 4 ppt). The model ensemble mean is  $1.37 \times 10^4 \text{ km}^3$ , within the range of these estimations.

## 2. Solid FW variability and trend

- The models can reproduce the observed interannual and seasonal variability of sea ice transport at Fram Strait. They simulated the large sea ice export events in the 1960s, 1980s and 1990s which caused the GSAs reported by (Dickson et al., 1988; Hakkinen, 2002) (Figure 11). They also well represented the observed variability of sea ice export described by Vinje et al. (1998); Kwok and Rothrock (1999); Kwok et al. (2004) (Figure 10). By referring to the observation reported by Spreen et al. (2009), Haine et al. (2015) suggest that the solid FW export at Fram Strait has declined by  $400 \text{ km}^3/\text{year}$  in the period 2000-2010 (compared to the climatological value of  $2300 \pm 340 \text{ km}^3/\text{year}$ ), a reduction at the level of interannual variability. The simulated decline of Fram Strait solid FW flux after 2000 in the model ensemble mean is similar to this synthesized value.
- The model ensemble means captured the observed upward changes of sea ice export at Davis Strait from 2005 to 2007 (Curry et al., 2014) and at the BKN from 1999/2000 to 2002/2003 (Kwok et al., 2005) (Figure 11).
- Due to lacking continuous sea ice thickness observations, there are no time series of solid FW storage that can be directly used to assess model results. Assimilation of sea ice concentration is used by PIOMAS to improve sea ice thickness simulations (Zhang and Rothrock, 2003). The time series of NH sea ice FWC based on the PIOMAS sea ice volume reanalysis (Schweiger et al., 2011) is shown in Figure 18. Both the interannual and seasonal variations are very consistent between the CORE-II model ensemble mean and the PIOMAS result. However, PIOMAS shows a steeper decline in the last few years than the model ensemble mean. The CORE-II models did not adequately reproduce the observed acceleration in the thinning trend after 2003 (Figure 13), which can explain their lower descending trend in sea ice volume compared to the PIOMAS result.

## 4. Conclusion

In this work we assessed the Arctic Ocean in 14 models participating in the Coordinated Ocean-ice Reference Experiments, phase II (CORE-II) intercomparison project. All the models are global and the ocean-sea ice components of respective climate models (Danabasoglu et al., 2014). They used the same atmospheric forcing data sets and bulk formula following the CORE-II protocol (Griffies et al.,

2012). The atmospheric forcing covers 60 years from 1948 to 2007 (Large and Yeager, 2009), and the models are run for 300 years corresponding to 5 consecutive loops of the 60-year forcing period. Model configurations including resolution, parameterization, parameters are decided by the model developing groups. In this paper we focus on the Arctic sea ice extent and the sources and storage of Arctic solid freshwater (FW).

The states of the model ensemble means are summarized at the end of each section. Other key points are itemized below.

#### 1. Sea ice extent and concentration

- Although there is a large spread in the Northern Hemisphere mean sea ice extent in the models, its interannual and seasonal variability is largely consistent with the observation (Figures 2 and 5).
- On average the descending trends in sea ice extent in the period of satellite observation is better simulated for September than for March. Except for four models that have too low sea ice extent, the September descending trend tends to be weaker in models with higher sea ice extent and thickness.
- The models consistently show good correlation between the sea ice extent in Barents Sea and the heat transport through the Barents Sea Opening (BSO) at 0 - 1 year lag (heat transport lead, Figure 6), as suggested in previous studies (Arthun et al., 2012).

#### 2. Solid FW budget

- There is large spread in mean sea ice thickness and volume in the models. In both March and September, models with thicker sea ice tend to have larger sea ice volume, except for the four models which have too thin sea ice (Figure 9). The model spread in sea ice volume can largely be explained by the spread in sea ice thickness.
- The models obtained descending trend in sea ice volume over the last 30 years, but there is a spread in the descending rate. The rate is mainly determined by the strength of the descending trend in sea ice thickness (Figure 12). The interannual variability of sea ice volume can be explained by that of sea ice thickness more than sea ice extent. The semi-closed Arctic geometry naturally reduces the sea ice volume sensitivity to sea ice extent.
- Sea ice export through the gateways and the thermodynamic sea ice production tend to compensate each other on decadal time scales (Figure 15). The decreasing sea ice thermodynamic growth rate in the recent decades is accompanied by a reduction in the sea ice export.
- The models tend to underestimate the observed sea ice thinning trend, most significantly after 2003. It remains to see whether this common issue is related to the atmospheric forcing used in the simulations or due to some general model features.

Overall, the CORE-II models, driven by the same inter-annually varying atmospheric state, did not demonstrate qualitatively similar mean state in the Arctic Ocean, as also found for the North Atlantic (Danabasoglu et al., 2014). The variability of most of the characteristics we explored, is modelled more consistently than the mean state, which is also a conclusion of the CORE-II North Atlantic study (Danabasoglu et al., 2015). It is noticed that the model spread in the mean state is larger than the interannual variability magnitude for many of the diagnostics. When we evaluate the model ensemble means, it is found that both the variability and mean state are reasonably reproduced. These conclusions apply to both the solid FW shown in this paper and the liquid FW state presented in Wang and et al. (2015). It is shown that the CORE-II models tend to underestimate the descending trends in sea ice thickness and March sea ice extent. It is necessary for the model development groups to work on the common issues for the important roles played by sea ice in the climate system.

It is worth pointing out that not all the conclusions based on the CORE-II models can be directly transferred to their respective coupled climate models. For example, the NCAR model is one of the models with very low sea ice thickness (Figure 8), but it has much thicker sea ice in the coupled climate model (CCSM4) simulation for the late 20th century, using the same model resolution and parameters

680 (Jahn et al., 2012b)<sup>8</sup>. Therefore the results presented in this work should be interpreted with caution when the context is extended to coupled models.

In this work we focused on the discussion of difference and similarity between the results of CORE-II simulations and observations, and tried to provide information on common issues and possible linkages between different key diagnostics used in the discussion. Such information can be helpful for further  
 685 improving models, but dedicated studies of model sensitivity to physical and numerical parameters are necessary in order to reduce model uncertainties identified through model intercomparisons.

## Acknowledgements

The WCRP/CLIVAR Ocean Model Development Panel (OMDP) is responsible for organising the Coordinated Ocean-sea ice Reference Experiments, with support from the international CLIVAR and  
 690 U.S. CLIVAR project offices. We are grateful for the efforts of modellers who have contributed to the simulation and processing of the CORE-II experiments. We thank Randi Ingvaldsen for providing us with the ocean transport data at the Barents Sea Opening. Comments by two reviewers and Claudia Wekerle, Richard Greatbatch and Tor Eldevik helped to improve the manuscript. AWI is a member of the Helmholtz Association of German Research Centers. Q. Wang is funded by the Helmholtz Climate  
 695 Initiative REKLIM (Regional Climate Change) project. C. Roth was supported by the Co-Operative Project RACE-Regional Atlantic Circulation and Global Change funded by the German Federal Ministry for Education and Research (BMBF), grant no. 03F0651B. The BERGEN contribution is supported by the Research Council of Norway through the EarthClim (207711/E10) and NOTUR/NorStore projects, as well as the Centre for Climate Dynamics at the Bjerknnes Centre for Climate Research. The CMCC  
 700 contribution received funding from the Italian Ministry of Education, University, and Research and the Italian Ministry of Environment, Land, and Sea under the GEMINA project. NCAR is sponsored by the U. S. National Science Foundation (NSF). S.G. Yeager was supported by the NOAA Climate Program Office under Climate Variability and Predictability Program Grant NA09OAR4310163 and NA13OAR4310138 and by the NSF Collaborative Research EaSM2 grant OCE-1243015 to NCAR. The  
 705 AWI-FESOM and Kiel-ORCA05 experiments were performed at the North-German Supercomputing Alliance (HLRN).

## Appendix A. Definition of freshwater content and transport

The freshwater content (FWC) is the amount of zero-salinity water required to be taken out from the ocean (or sea ice) so that its salinity is changed to the chosen reference salinity. The Arctic liquid FWC is calculated as

$$\iiint_{\Omega} \frac{S_{ref} - S_o}{S_{ref}} dV \quad (1)$$

where the 3D integration is taken over the whole Arctic domain  $\Omega$  in this study,  $S_o$  is ocean salinity, and  $S_{ref} = 34.8$  is the reference salinity. This value is widely used in studies on Arctic freshwater (e.g., Aagaard and Carmack, 1989; Serreze et al., 2006; Haine et al., 2015). We also compare the vertically integrated FWC at each horizontal grid cell, which is

$$\int_D^{surface} \frac{S_{ref} - S_o}{S_{ref}} dh \quad (2)$$

where  $D$  is the uppermost depth where the ocean salinity is equal to the reference salinity. Because we  
 710 plan to compare the spatial distribution of near surface freshwater and its change over recent years, we do not consider the water mass saltier than the reference salinity.

---

<sup>8</sup>Simulated sea ice thickness can be significantly influenced by the choice of albedos. At NCAR, the same albedos were used for both the fully-coupled model simulations and the CORE-II experiments. The albedos were partly adjusted to help tune the top-of-the-atmosphere heat flux in the coupled pre-industrial control simulation. With the chosen albedos, the simulated sea ice thickness in the coupled simulation is very reasonable, while it is underestimated in the CORE-II simulation.

Liquid freshwater transport through a gateway is defined as

$$\iint_S \frac{S_{ref} - S_o}{S_{ref}} v_n ds \quad (3)$$

where the integration is taken over the vertical section area  $S$ ,  $v_n$  is the ocean velocity normal to the transect. Equation 3 can be written as

$$\iint_S \frac{S_{ref} - S_o}{S_{ref}} v_n ds = \iint_S v_n ds - \frac{1}{S_{ref}} \iint_S S_o v_n ds \quad (4)$$

On the right hand side, the first term is ocean volume transport and the second term is salt transport normalized by the reference salinity.

The Arctic sea ice freshwater content is defined as

$$\iint_A \frac{S_{ref} - S_i}{S_{ref}} \frac{\rho_i}{\rho_o} h_i ds \quad (5)$$

where the integration is taken over the Arctic surface area  $A$ ,  $h_i$  is the effective sea ice thickness (mean thickness in a grid cell),  $\rho_o$  is the reference ocean density (in the model it is used for the volume conversion between water and sea ice),  $\rho_i$  is the sea ice density.

The Arctic sea ice freshwater transport through a transect is defined as

$$\iint_L \frac{S_{ref} - S_i}{S_{ref}} \frac{\rho_i}{\rho_o} h_i v_i dl \quad (6)$$

where the integration is taken over the section line  $L$ ,  $v_i$  is the ice drift velocity normal to the transect. Snow freshwater content and transport are defined similarly by using snow effective thickness, salinity and density. Total solid freshwater transport is the sum of sea ice and snow freshwater transports.

## Appendix B. Model spinup

In the analysis of the CORE-II models for the North Atlantic, it was shown that 5 loops are sufficient for more than half of the models to reach equilibrium with respect to a key diagnostic, the Atlantic Meridional Overturning Circulation (AMOC) maximum (Danabasoglu et al., 2014). Here we will examine if the models achieved equilibrium in the Arctic Ocean. We choose two important diagnostics to evaluate the spinup of the ocean: the liquid freshwater content (FWC) and the total liquid freshwater (FW) flux from the Arctic Ocean to the subpolar North Atlantic. The concept and definition of FWC and FW fluxes are given in Section 1.2 and Appendix A.

Figure 19a shows the liquid FWC time series for the 300 years simulations. As all models start from the climatological hydrography, the liquid FWCs in different models are quite similar at the beginning. They increase rapidly during the first model loop in most of the models, and the most rapid increase takes place during the first decade. Although the FWCs have increasing tendency in the first few decades, they decrease in four models after the increasing phase, including NCAR, GFDL-MOM, NOC and Kiel-ORCA05. Among these models the NCAR model starts to show descending trend the earliest, after about 30 model years.

We take the same measure as in the AMOC CORE-II paper (Danabasoglu et al., 2014) to illustrate whether the models reach equilibrium at the end of the experiments. The root-mean-square (RMS) difference and the correlation coefficients between two sequential loops are calculated and shown in Figure 20a. The RMS difference is normalized by the mean FWC of all models. The RMS difference drops quickly during the first three loops. Except for Kiel-ORCA05 and GFDL-MOM, which have increasing RMS difference after the third loop, other models have RMS difference less than 5% of the ensemble mean liquid FWC at the end. The correlation between sequential loops increases with time on average, although most of the models show oscillations in the magnitude of the correlation coefficients. Except for FSU-HYCOM, which has a significant drop with the correlation coefficient, the models have correlation coefficients larger than 0.9 at the end.

Another quantity we choose to check for equilibrium is the total liquid FW transport from the Arctic Ocean to the North Atlantic. The sum of the FW fluxes through Fram and Davis Straits is plotted in

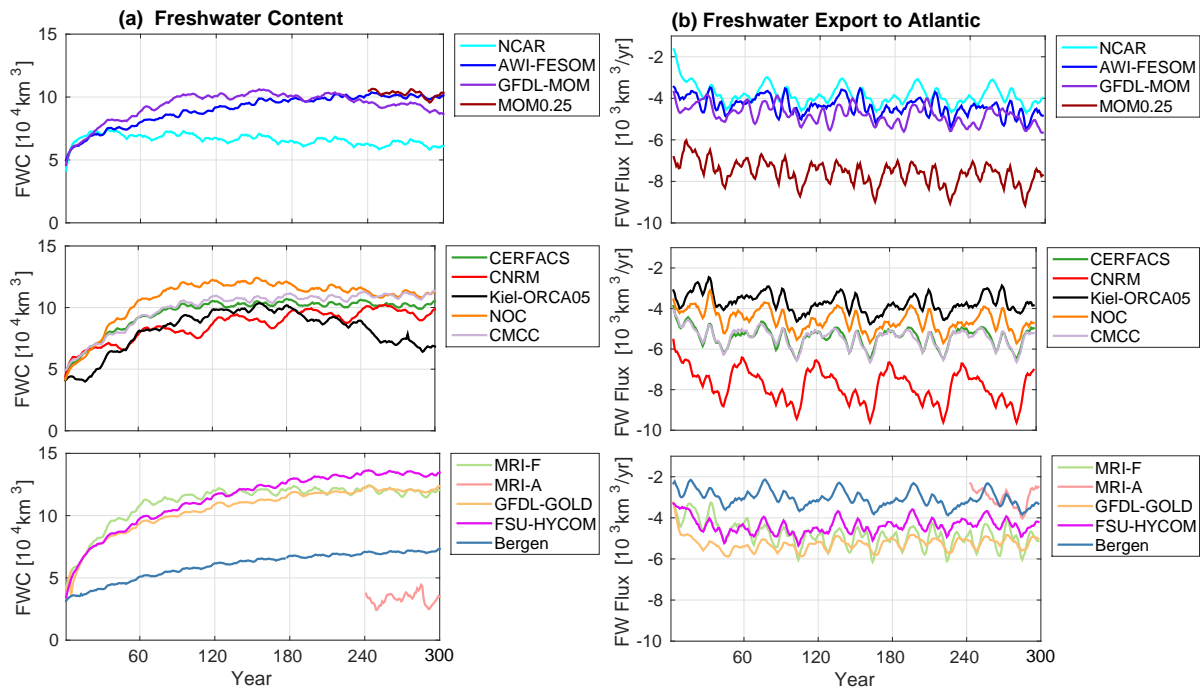
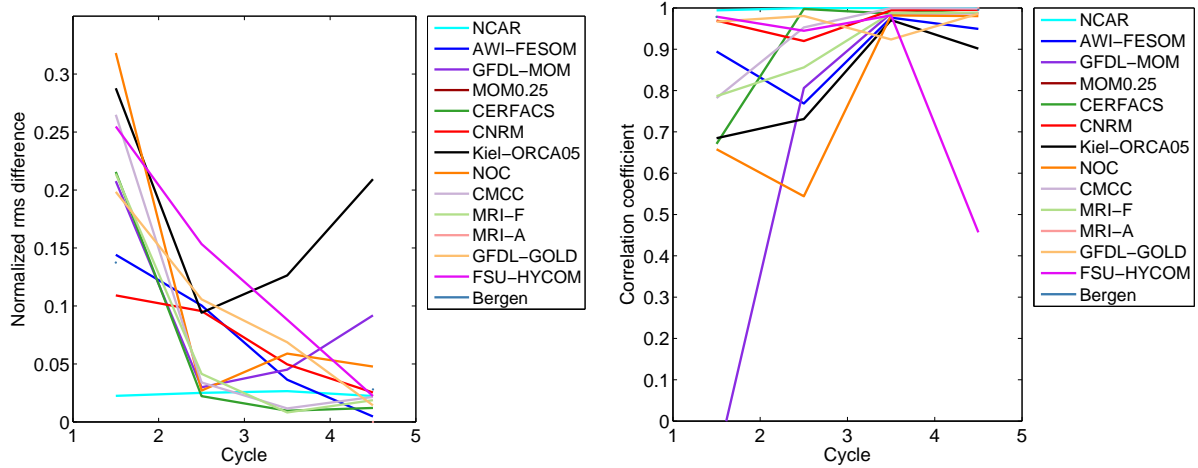


Figure 19: (a) Annual mean Arctic liquid freshwater content (FWC) for the entire 300-yr integration length. (b) Five years running mean Arctic freshwater (FW) export fluxes to the North Atlantic, that is, the sum of FW fluxes through Davis Strait and Fram Strait. Each 60-yr loop, corresponding to calendar years 1948-2007, is indicated by the vertical grid lines. FWC data for MOM0.25 is only available for the last loop. The MRI-A experiment is only done for the last loop, which starts after a 10 years transition simulation from the end of the MRI-F 4th loop. Bergen FWC data are missing for a few years in the 4th loop.

(a) Liquid freshwater content



(b) Liquid freshwater transport

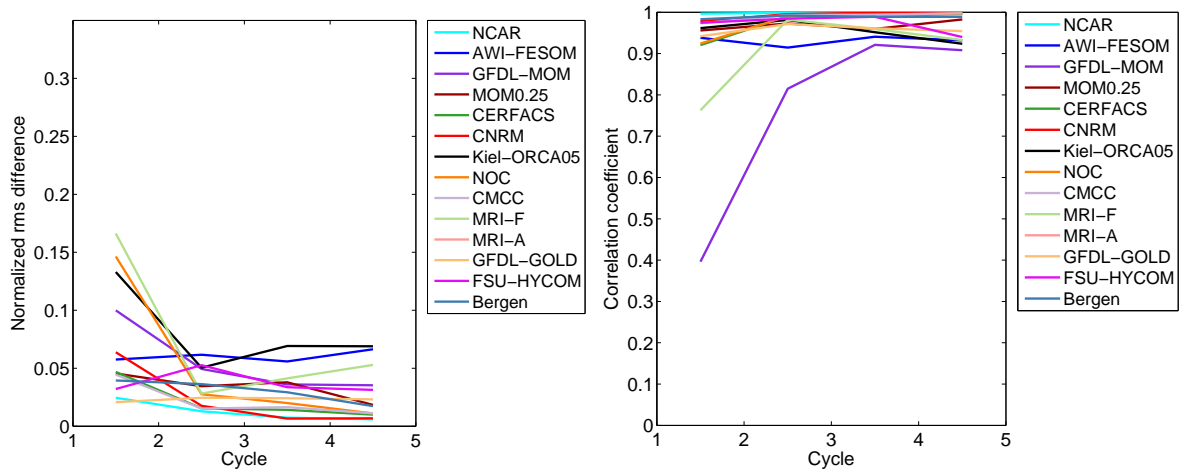


Figure 20: Convergence of (a) Arctic freshwater content and (b) freshwater export to the North Atlantic. Left (right) panels show the RMS difference (correlation coefficients) between two consecutive loops. The period of 1978 - 2007 in each loop is used in the calculation. Results for a few models are missing for the reasons mentioned in the caption of Figure 19.

Figure 19b. Although the models have very large spread in the magnitude of liquid FW transport, they do not have substantial descending or ascending trend throughout the 300 years simulations. The model convergence with respect to the liquid FW fluxes is shown in Figure 20b. On average, the normalized RMS difference between the first two loops is smaller than that for the liquid FWC, and reaches quasi-equilibrium faster. The correlation between sequential loops for the liquid freshwater flux is more than 0.9 throughout the experiments for all models except for GFDL-MOM and MRI-F, which have low values for the first few loops.

As indicated by the convergence of Arctic liquid FWC and FW transport, most of the models can reach equilibrium within 5 loops. Convergence analysis was also made for solid FWC and FW transport, and they show better convergence than their liquid counterparts (not shown).

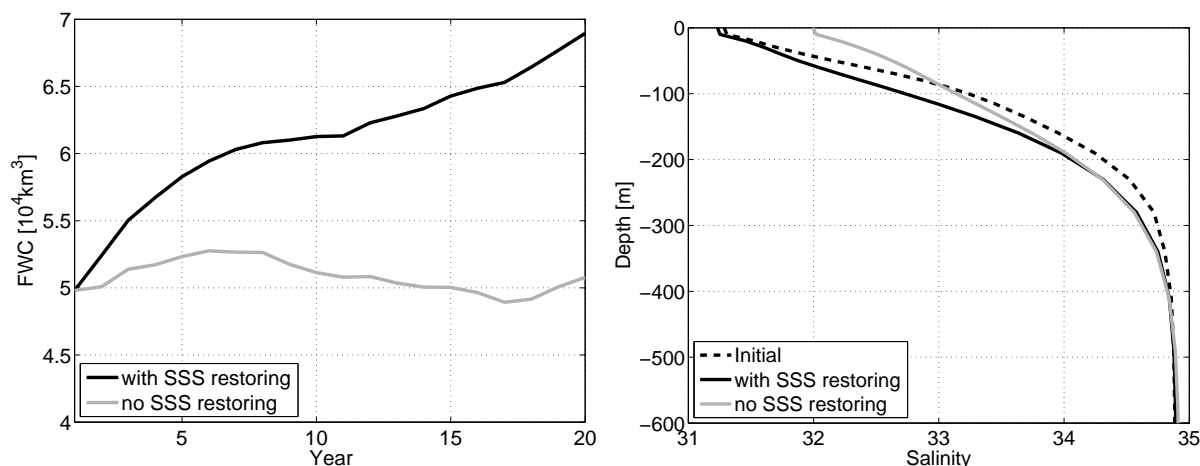


Figure 21: (left) Annual mean liquid FWC simulated in FESOM. The time series compare the FWC in two simulations when sea surface salinity (SSS) restoring is switched on and off. (right) Zonal mean salinity profiles averaged in the Arctic basin at the beginning of the simulations (dashed line) and after 20 years (solid lines).

All the models (except for the one with ocean assimilation) tend to simulate a much fresher Arctic Ocean than that suggested by climatological hydrography. Such a similar model behaviour indicates a possible common cause. We carried out one sensitivity experiment with FESOM to better understand the process related to the simulated liquid FWC trend. In this experiment we switched off the sea surface salinity (SSS) restoring and ran the model for 20 years starting from climatological hydrography. When SSS restoring is switched off, the rapid increasing trend of FWC disappears (Figure 21(left)). In the case without SSS restoring, the model has a positive salinity drift near the ocean surface and a negative drift between about 100 – 400 m depth (Figure 21(right)). When the SSS restoring is switched on, it corrects the near surface salinity drift and the surface salinity is maintained close to the climatology as expected. This correction acts effectively to increase the volume-integrated FWC.

Nguyen et al. (2009) proposed an explanation for model salinity drift in Arctic Ocean following the experience for the Southern Ocean described by Duffy et al. (1999). They found that if salt rejected during ice formation is added to the ocean at the surface, the static instability in the model will initialize strong vertical mixing and weaken the vertical salinity gradient, resulting in negative salinity anomaly in the halocline and positive salinity anomaly at the ocean surface. By distributing rejected salt in the ocean column with some vertical distribution function and reducing the vertical mixing coefficient, they got significantly improved salinity profiles. It remains to see if the common issue of upper ocean salinity drift and FWC trend in the CORE-II models can be alleviated when adequate parameterizations of salt rejection are used.

The Arctic Ocean is not only a reservoir of FW, but also a northern terminate of North Atlantic Current, which brings saltier Atlantic Water to the Arctic Ocean. Therefore the total Arctic liquid FWC can also be influenced by the Atlantic inflow. Arctic liquid FW and Atlantic Water circulation in the Arctic Ocean simulated by the CORE-II models are discussed by Wang and et al. (2015) and Ilicak and et al. (2015), respectively. Here we just mention that the descending trend of liquid FWC in the last two loops in Kiel-ORCA05 (Figure 19a) can be explained by the Atlantic Water inflow, which is associated

with an upward trend in its simulated AMOC during the last decades (see the CORE-II North Atlantic results described by Danabasoglu et al., 2014).

## References

- 785 Agaard, K., Carmack, E.C., 1989. The role of sea ice and other fresh-water in the Arctic circulation. *J. Geophys. Res.* 94, 14485–14498.
- Agaard, K., Swift, J.H., Carmack, E., 1985. Thermohaline circulation in the Arctic mediterranean seas. *Journal of Geophysical Research-oceans* 90, 4833–4846.
- Arthun, M., Eldevik, T., Smedsrud, L.H., Skagseth, O., Ingvaldsen, R.B., 2012. Quantifying the Influence of Atlantic Heat on Barents Sea Ice Variability and Retreat. *Journal of Climate* 25, 4736–4743.
- 790 Bhatt, U.S., Walker, D.A., Walsh, J.E., Carmack, E.C., Frey, K.E., Meier, W.N., Moore, S.E., Parmentier, F.J.W., Post, E., Romanovsky, V.E., Simpson, W.R., 2014. Implications of Arctic sea ice decline for the Earth System. *Annual Review of Environment and Resources* 39, 57–89.
- Cavaliere, D.J., Parkinson, C.L., 2012. Arctic sea ice variability and trends, 1979-2010. *Cryosphere* 6, 881–889.
- 795 Comiso, J.C., 2012. Large decadal decline in the Arctic multiyear ice cover. *J. Clim.* 25, 1176–1193.
- Comiso, J.C., Nishio, F., 2008. Trends in the sea ice cover using enhanced and compatible AMSR-E, SSM/I, and SMMR data. *J. Geophys. Res.- Oceans* 113, C02S07.
- Comiso, J.C., Parkinson, C.L., Gersten, R., Stock, L., 2008. Accelerated decline in the Arctic sea ice cover. *Geophys. Res. Lett.* 35, L01703.
- 800 Curry, B., Lee, C.M., Petrie, B., Moritz, R.E., Kwok, R., 2014. Multiyear volume, liquid freshwater, and sea ice transports through Davis Strait, 2004-2010. *Journal of Physical Oceanography* 44, 1244–1266.
- Danabasoglu, G., Yeager, S.G., Bailey, D., Behrens, E., Bentsen, M., Bi, D., Biastoch, A., Böning, C., Bozec, A., Canuto, V.M., Cassou, C., Chassignet, E., Coward, A.C., Danilov, S., Diansky, N., Drange, H., Farneti, R., Fernandez, E., Fogli, P.G., Forget, G., Fujii, Y., Griffies, S.M., Gusev, A., Heimbach, P., Howard, A., Jung, T., Kelley, M., Large, W.G., Leboissetier, A., Lu, J., Madec, G., Marsland, S.J., Masina, S., Navarra, A., Nurser, A.G., Pirani, A., y Melia, D.S., Samuels, B.L., Scheinert, M., Sidorenko, D., Treguier, A.M., Tsujino, H., Uotila, P., Valcke, S., Voldoire, A., Wang, Q., 2014. North Atlantic simulations in Coordinated Ocean-ice Reference Experiments phase {II} (CORE-II). part i: Mean states. *Ocean Modelling* 73, 76 – 107.
- 810 Danabasoglu, G., Yeager, S.G., Bailey, D., Behrens, E., Bentsen, M., Bi, D., Biastoch, A., Böning, C., Bozec, A., Canuto, V.M., Cassou, C., Chassignet, E., Coward, A.C., Danilov, S., Diansky, N., Drange, H., Farneti, R., Fernandez, E., Fogli, P.G., Forget, G., Fujii, Y., Griffies, S.M., Gusev, A., Heimbach, P., Howard, A., Jung, T., Kelley, M., Large, W.G., Leboissetier, A., Lu, J., Madec, G., Marsland, S.J., Masina, S., Navarra, A., Nurser, A.G., Pirani, A., y Melia, D.S., Samuels, B.L., Scheinert, M., Sidorenko, D., Treguier, A.M., Tsujino, H., Uotila, P., Valcke, S., Voldoire, A., Wang, Q., 2015. North Atlantic simulations in Coordinated Ocean-ice Reference Experiments phase {II} (CORE-II). part ii: Inter-annual to decadal variability. *Ocean Modelling*, submitted.
- 820 Dickson, R., Meincke, J., Malmberg, S., Lee, A.J., 1988. The Great Salinity Anomaly In the Northern North-atlantic 1968-1982. *Progress In Oceanography* 20, 103–151.
- Dickson, R., Rudels, B., Dye, S., Karcher, M., Meincke, J., Yashayaev, I., 2007. Current estimates of freshwater flux through Arctic and subarctic seas. *Prog. Oceanogr.* 73, 210–230.
- Dickson, R.R., Osborn, T.J., Hurrell, J.W., Meincke, J., Blindheim, J., Adlandsvik, B., Vinje, T., Alekseev, G., Maslowski, W., 2000. The Arctic Ocean Response to the North Atlantic Oscillation. *J. Climate* 13, 2671 – 2696.

- 825 Duffy, P.B., Eby, M., Weaver, A.J., 1999. Effects of sinking of salt rejected during formation of sea ice on results of an ocean-atmosphere-sea ice climate model. *Geophysical Research Letters* 26, 1739–1742.
- Fetterer, F., Knowles, K., Meier, W., M., S., 2002. *Sea Ice Index*. Boulder, Colorado USA: National Snow and Ice Data Center. Digital media , updated daily.
- Goosse, H., Fichefet, T., Campin, J.M., 1997. The effects of the water flow through the Canadian Archipelago in a global ice-ocean model. *Geophysical Research Letters* 24, 1507–1510.
- 830 Griffies, S., Winton, M., Samuels, B., Danabasoglu, G., Yeager, S., Marlsand, S., Drange, H., Bentsen, M., 2012. Datasets and protocol for the CLIVAR WGOMD Coordinated Ocean-sea ice Reference Experiments (COREs). Technical Report 21. WCRP Report.
- Griffies, S.M., Biastoch, A., Böning, C., Bryan, F., Danabasoglu, G., Chassignet, E.P., England, M.H., Gerdes, R., Haak, H., Hallberg, R.W., Hazeleger, W., Jungclaus, J., Large, W.G., Madec, G., Pirani, A., Samuels, B.L., Scheinert, M., Gupta, A.S., Severijns, C.A., Simmons, H.L., Treguier, A.M., Winton, M., Yeager, S., Yin, J., 2009. Coordinated Ocean-ice Reference Experiments (COREs). *Ocean Modell.* 26, 1–46.
- 840 Haak, H., Jungclaus, J., Mikolajewicz, U., Latif, M., 2003. Formation and propagation of great salinity anomalies. *Geophysical Research Letters* 30, 1473.
- Haine, T., Curry, B., Gerdes, R., Hansen, E., Karcher, M., Lee, C., Rudels, B., Spreen, G., de Steur, L., Stewart, K., Woodgate, R., 2015. Arctic freshwater export: Status, mechanisms, and prospects. *Global and Planetary Change* 125, 13 – 35.
- Hakkinen, S., 1999. A simulation of thermohaline effects of a great salinity anomaly. *Journal of Climate* 845 12, 1781–1795.
- Hakkinen, S., 2002. Freshening of the Labrador Sea surface waters in the 1990s: Another great salinity anomaly? *Geophysical Research Letters* 29, 2232.
- Holland, M.M., Finnis, J., Barrett, A.P., Serreze, M.C., 2007. Projected changes in Arctic Ocean freshwater budgets. *Journal of Geophysical Research-biogeosciences* 112, G04S55.
- 850 Holloway, G., Dupont, F., Golubeva, E., Haekkinen, S., Hunke, E., Jin, M., Karcher, M., Kauker, F., Maltrud, M., Maqueda, M.A.M., Maslowski, W., Platov, G., Stark, D., Steele, M., Suzuki, T., Wang, J., Zhang, J., 2007. Water properties and circulation in Arctic Ocean models. *Journal of Geophysical Research-oceans* 112, C04S03.
- Ilicak, M., et al., 2015. An assessment of the arctic ocean hydrography in a suite of interannual core-ii simulations. *Ocean Modell.* , under revision.
- 855 Jahn, A., Aksenov, Y., de Cuevas, B.A., de Steur, L., Hakkinen, S., Hansen, E., Herbaut, C., Houssais, M.N., Karcher, M., Kauker, F., Lique, C., Nguyen, A., Pemberton, P., Worthen, D., Zhang, J., 2012a. Arctic Ocean freshwater: How robust are model simulations? *J. Geophys. Res. - Oceans* 117, C00D16.
- Jahn, A., Sterling, K., Holland, M.M., Kay, J.E., Maslanik, J.A., Bitz, C.M., Bailey, D.A., Stroeve, J., Hunke, E.C., Lipscomb, W.H., Pollak, D.A., 2012b. Late-Twentieth-Century Simulation of Arctic Sea Ice and Ocean Properties in the CCSM4. *Journal of Climate* 25, 1431–1452.
- 860 Johnson, M., Gaffigan, S., Hunke, E., Gerdes, R., 2007. A comparison of Arctic Ocean sea ice concentration among the coordinated AOMIP model experiments. *Journal of Geophysical Research-Oceans* 112, C04S11.
- 865 Johnson, M., Proshutinsky, A., Aksenov, Y., Nguyen, A.T., Lindsay, R., Haas, C., Zhang, J., Diansky, N., Kwok, R., Maslowski, W., Haekkinen, S., Ashik, I., de Cuevas, B., 2012. Evaluation of Arctic sea ice thickness simulated by Arctic Ocean Model Intercomparison Project models. *Journal of Geophysical Research-oceans* 117, C00D13.
- 870 Jungclaus, J.H., Haak, H., Latif, M., Mikolajewicz, U., 2005. Arctic-North Atlantic interactions and multidecadal variability of the meridional overturning circulation. *Journal of Climate* 18, 4013–4031.

- Karcher, M., Beszczynska-Moeller, A., Kauker, F., Gerdes, R., Heyen, S., Rudels, B., Schauer, U., 2011. Arctic Ocean warming and its consequences for the Denmark Strait overflow. *Journal of Geophysical Research-oceans* 116, C02037.
- Karcher, M., Kauker, F., Gerdes, R., Hunke, E., Zhang, J., 2007. On the dynamics of Atlantic Water circulation in the Arctic Ocean. *J. Geophys. Res. - Oceans* 112, C04S02.
- Köberle, C., Gerdes, R., 2003. Mechanisms determining the variability of Arctic sea ice conditions and export. *Journal of Climate* 16, 2843–2858.
- Koenigk, T., Brodeau, L., Graverson, R., Karlsson, J., Svensson, G., Tjernström, M., Willén, U., Wyser, K., 2013. Arctic climate change in 21st century CMIP5 simulations with EC-Earth. *Climate Dynamics* 40, 2719–2743.
- Koenigk, T., Mikolajewicz, U., Haak, H., Jungclaus, J., 2006. Variability of Fram Strait sea ice export: causes, impacts and feedbacks in a coupled climate model. *Climate Dynamics* 26, 17–34.
- Kwok, R., 2007. Baffin Bay ice drift and export: 2002-2007. *Geophysical Research Letters* 34, L19501.
- Kwok, R., 2009. Outflow of Arctic Ocean Sea Ice into the Greenland and Barents Seas: 1979-2007. *Journal of Climate* 22, 2438–2457.
- Kwok, R., Cunningham, G.F., Pang, S.S., 2004. Fram Strait sea ice outflow. *Journal of Geophysical Research-oceans* 109, C01009.
- Kwok, R., Cunningham, G.F., Wensnahan, M., Rigor, I., Zwally, H.J., Yi, D., 2009. Thinning and volume loss of the Arctic Ocean sea ice cover: 2003-2008. *Journal of Geophysical Research-oceans* 114, C07005.
- Kwok, R., Maslowski, W., Laxon, S.W., 2005. On large outflows of Arctic sea ice into the Barents Sea. *Geophysical Research Letters* 32, L22503.
- Kwok, R., Rothrock, D.A., 1999. Variability of Fram Strait ice flux and North Atlantic Oscillation. *Journal of Geophysical Research-oceans* 104, 5177–5189.
- Kwok, R., Rothrock, D.A., 2009. Decline in arctic sea ice thickness from submarine and icesat records: 1958-2008. *Geophysical Research Letters* 36, L15501.
- Large, W.G., Yeager, S.G., 2009. The global climatology of an interannually varying air-sea flux data set. *Climate Dynamics* 33, 341–364.
- Laxon, S., Peacock, N., Smith, D., 2003. High interannual variability of sea ice thickness in the Arctic region. *Nature* 425, 947–950.
- Laxon, S.W., Giles, K.A., Ridout, A.L., Wingham, D.J., Willatt, R., Cullen, R., Kwok, R., Schweiger, A., Zhang, J., Haas, C., Hendricks, S., Krishfield, R., Kurtz, N., Farrell, S., Davidson, M., 2013. CryoSat-2 estimates of Arctic sea ice thickness and volume. *Geophys. Res. Lett.* 40, 732–737.
- Nguyen, A.T., Menemenlis, D., Kwok, R., 2009. Improved modeling of the Arctic halocline with a subgrid-scale brine rejection parameterization. *J. Geophys. Res. - Oceans* 114, C11014.
- Parkinson, C.L., Cavalieri, D.J., 2008. Arctic sea ice variability and trends, 1979-2006. *Journal of Geophysical Research-oceans* 113, C07003.
- Parkinson, C.L., Cavalieri, D.J., Gloersen, P., Zwally, H.J., Comiso, J.C., 1999. Arctic sea ice extents, areas, and trends, 1978-1996. *Journal of Geophysical Research-oceans* 104, 20837–20856.
- Proshutinsky, A., Aksenov, Y., Kinney, J.C., Gerdes, R., Golubeva, E., Holland, D., Holloway, G., Jahn, A., Johnson, M., Popova, E., Steele, M., Watanabe, E., 2011. Recent Advances in Arctic Ocean Studies Employing Models from the Arctic Ocean Model Intercomparison Project. *Oceanography* 24, 102–113.

- Rampal, P., Weiss, J., Dubois, C., Campin, J., 2011. Iccc climate models do not capture Arctic sea ice drift acceleration: Consequences in terms of projected sea ice thinning and decline. *J. Geophys. Res.* 116, C00D07.
- Rawlins, M.A., Steele, M., Holland, M.M., Adam, J.C., Cherry, J.E., Francis, J.A., Groisman, P.Y., Hinzman, L.D., Huntington, T.G., Kane, D.L., Kimball, J.S., Kwok, R., Lammers, R.B., Lee, C.M., Lettenmaier, D.P., McDonald, K.C., Podest, E., Pundsack, J.W., Rudels, B., Serreze, M.C., Shiklomanov, A., Skagseth, O., Troy, T.J., Voeroesmart, C.J., Wensnahan, M., Wood, E.F., Woodgate, R., Yang, D., Zhang, K., Zhang, T., 2010. Analysis of the Arctic system for freshwater cycle intensification: Observations and expectations. *Journal of Climate* 23, 5715–5737.
- Rothrock, D.A., Percival, D.B., Wensnahan, M., 2008. The decline in Arctic sea-ice thickness: Separating the spatial, annual, and interannual variability in a quarter century of submarine data. *J. Geophys. Res.* 113, C05003.
- Rothrock, D.A., Yu, Y., Maykut, G.A., 1999. Thinning of the Arctic sea-ice cover. *Geophysical Research Letters* 26, 3469–3472.
- Rudels, B., Friedrich, H., 2000. The transformation of the Atlantic Water in the Arctic Ocean and their significance for the freshwater budget, in: Lewis, E.L.e.a. (Ed.), *The Freshwater Budget of the Arctic Ocean*. Kluwer, pp. 503–532.
- Schweiger, A., Lindsay, R., Zhang, J., Steele, M., Stern, H., Kwok, R., 2011. Uncertainty in modeled Arctic sea ice volume. *Journal of Geophysical Research-oceans* 116, C00D06.
- Serreze, M.C., Barrett, A.P., Slater, A.G., Woodgate, R.A., Aagaard, K., Lammers, R.B., Steele, M., Moritz, R., Meredith, M., Lee, C.M., 2006. The large-scale freshwater cycle of the Arctic. *J. Geophys. Res. - Oceans* 111, C11010.
- Serreze, M.C., Barry, R.G., 2011. Processes and impacts of Arctic amplification: A research synthesis. *Global and Planetary Change* 77, 85–96.
- Serreze, M.C., Holland, M.M., Stroeve, J., 2007. Perspectives on the Arctic’s shrinking sea-ice cover. *Science* 315, 1533–1536.
- Smedsrud, L.H., Esau, I., Ingvaldsen, R.B., Eldevik, T., Haugan, P.M., Li, C., Lien, V.S., Olsen, A., Omar, A.M., Ottera, O.H., Risebrobakken, B., Sando, A.B., Semenov, V.A., Sorokina, S.A., 2013. The role of the Barents Sea in the Arctic climate system. *Reviews of Geophysics* 51, 415–449.
- Spren, G., Kern, S., Stammer, D., Hansen, E., 2009. Fram Strait sea ice volume export estimated between 2003 and 2008 from satellite data. *Geophys. Res. Lett.* 36, L19502.
- Stroeve, J., Serreze, M., Drobot, S., Gearheard, S., Holland, M., Maslanik, J., Meier, W., Scambos, T., 2008. Arctic sea ice extent plummets in 2007, AGU. pp. 13–14.
- Stroeve, J.C., Kattsov, V., Barrett, A., Serreze, M., Pavlova, T., Holland, M., Meier, W.N., 2012a. Trends in Arctic sea ice extent from CMIP5, CMIP3 and observations. *Geophysical Research Letters* 39, L16502.
- Stroeve, J.C., Serreze, M.C., Holland, M.M., Kay, J.E., Malanik, J., Barrett, A.P., 2012b. The arctic’s rapidly shrinking sea ice cover: a research synthesis. *Climatic Change* 110, 1005–1027.
- Vinje, T., 2001. Fram strait ice fluxes and atmospheric circulation: 1950-2000. *Journal of Climate* 14, 3508–3517.
- Vinje, T., Nordlund, N., Kvambekk, A., 1998. Monitoring ice thickness in Fram Strait. *Journal of Geophysical Research-oceans* 103, 10437–10449.
- Wadley, M.R., Bigg, G.R., 2002. Impact of flow through the Canadian Archipelago and Bering Strait on the north Atlantic and Arctic circulation: An ocean modelling study. *Quarterly Journal of the Royal Meteorological Society* 128, 2187–2203.

- 960 Wang, Q., et al., 2015. An assessment of the arctic ocean in a suite of interannual core-ii simulations.  
part ii: Liquid freshwater. *Ocean Modell.* , under revision.
- Wang, Q., Myers, P., Hu, X., Bush, A., 2012. Flow constraints on pathways through the Canadian Arctic Archipelago. *Atmosphere-ocean* 50, 373–385.
- Woodgate, R.A., Aagaard, K., 2005. Revising the Bering Strait freshwater flux into the Arctic Ocean. *Geophysical Research Letters* 32, L02602.
- 965 Zhang, J.L., Rothrock, D.A., 2003. Modeling global sea ice with a thickness and enthalpy distribution model in generalized curvilinear coordinates. *Monthly Weather Review* 131, 845–861.